PHYSIOLOGY

Remodeling p38 signaling in muscle controls locomotor activity via IL-15

Cintia Folgueira[1]*†, Leticia Herrera-Melle[1]†, Juan Antonio López[1,2], Victor Galvan-Alvarez[3,4], Marcos Martin-Rincon[3,4], María Isabel Cuartero[1,5], Alicia García-Culebras[1,6], Phillip A. Dumesic[7], Elena Rodríguez[1,8], Luis Leiva-Vega[1,8], Marta León[1,8], Begoña Porteiro[9,10], Cristina Iglesias[9,10], Jorge L. Torres[11], Lourdes Hernández-Cosido[12], Clara Bonacasa[1,8], Miguel Marcos[13], María Ángeles Moro[1], Jesús Vázquez[1,2], Jose A. L. Calbet[3,4,14], Bruce M. Spiegelman[7], Alfonso Mora[1,8]*, Guadalupe Sabio[1,8]*

Skeletal muscle has gained recognition as an endocrine organ releasing myokines upon contraction during physical exercise. These myokines exert both local and pleiotropic health benefits, underscoring the crucial role of muscle function in countering obesity and contributing to the overall positive effects of exercise on health. Here, we found that exercise activates muscle p38γ, increasing locomotor activity through the secretion of interleukin-15 (IL-15). IL-15 signals in the motor cortex, stimulating locomotor activity. This activation of muscle p38γ, leading to an increase locomotor activity, plays a crucial role in reducing the risk of diabetes and liver steatosis, unveiling a vital muscle-brain communication pathway with profound clinical implications. The correlation between p38γ activation in human muscle during acute exercise and increased blood IL-15 levels highlights the potential therapeutic relevance of this pathway in treating obesity and metabolic diseases. These findings provide valuable insights into the molecular basis of exercise-induced myokine responses promoting physical activity.

INTRODUCTION

Obesity is the most common metabolic disorder worldwide, with its incidence and prevalence rates continuing to rise, affecting over 650 million adults globally according to 2016 estimates (*1*). In the battle against the global epidemic of obesity-induced metabolic diseases, adopting a healthy lifestyle, including calorie restriction and regular exercise, has proven to be an effective strategy for prevention and treatment. While physical activity has been found to trigger intrinsic motivation for exercising (*2*), the precise molecular mechanisms underlying this muscle-brain interaction have not been fully determined. Recent evidence highlights the role of skeletal muscle as an endocrine organ that secretes various factors participating in interorgan communication (*3*). These secreted factors, collectively known as myokines, include protein hormones, small molecules, lipids, and other substances released from contracting skeletal muscle (*4*). It has been shown that exercise improves metabolic status because of not only its well-known effects on skeletal muscle metabolism but also by the secretion of myokines acting in distant organs (*5*). Understanding the role of these myokines and their secretion in response to exercise holds great promise in preventing obesity and associated metabolic disorders.

Alterations of skeletal muscle signaling can compromise metabolic homeostasis (*6*), and physical inactivity can disrupt the secretion of myokines (*7*). This disturbance in interorgan cross-talk can lead to various metabolic diseases, including chronic conditions like type 2 diabetes, cardiovascular disease, fatty liver disease, and cancer (*5*, *7*). Despite the notable benefits of exercise in the treatment and prevention of metabolic diseases, our understanding of the mechanisms through which exercise improves metabolic health remains limited. One of the pathways activated during intermittent or continuous exercise in human skeletal muscle is the p38 signaling pathway (*8*). Although p38 activation increases insulin-independent glucose uptake and oxidative metabolism in muscle during exercise, the same pathway promotes insulin resistance and glucose intolerance in metabolic syndrome (*9*). The contrasting effects of p38 activation in exercise and obesity may be attributed to the different functions of the four members of the p38 family: alpha, beta, gamma, and delta. Encoded by four separate genes with distinct tissue expression patterns (*10*), each p38 family member has the potential to induce specific responses in skeletal muscle; however, the individual contributions of p38s to the metabolic adaptation of skeletal muscle remain unclear. The impact of muscle-specific p38 deficiency on systemic metabolism is still unknown.

In this study, we revealed that exercise-induced activation of muscle p38γ leads to the production of interleukin-15 (IL-15), which subsequently enhances spontaneous physical activity. Furthermore, we observed the presence of this p38γ/IL-15 axis in humans after exercise, underscoring the relevance of this signaling pathway, which

[1]Centro Nacional de Investigaciones Cardiovasculares (CNIC), Madrid, Spain. [2]CIBER de Enfermedades Cardiovasculares (CIBERCV), Madrid, Spain. [3]Department of Physical Education, University of Las Palmas de Gran Canaria, Campus Universitario de Tafira s/n, Las Palmas de Gran Canaria 35017, Spain. [4]Research Institute of Biomedical and Health Sciences (IUIBS), University of Las Palmas de Gran Canaria, Canary Islands, Spain. [5]Unidad de Investigación Neurovascular, Departamento de Farmacología y Toxicología, Facultad de Medicina, Universidad Complutense de Madrid (UCM), Madrid, Spain. [6]Departamento de Biología Celular, Facultad de Medicina, Universidad Complutense de Madrid (UCM), Madrid, Spain. [7]Dana Farber Cancer Institute (DFCI), Department of Cell Biology, Harvard University Medical School, Boston, MA, USA. [8]Centro Nacional de Investigaciones Oncológicas (CNIO), Madrid, Spain. [9]Department of Physiology, CiMUS, University of Santiago de Compostela-Instituto de Investigación Sanitaria, Santiago de Compostela 15782, Spain; [10]CIBER Fisiopatología de la Obesidad y Nutrición (CIBERobn), 15706 Santiago de Compostela, Spain. [11]Complejo Asistencial de Zamora, Zamora, Spain. [12]Bariatric Surgery Unit, Department of General Surgery, University Hospital of Salamanca, Department of Surgery, University of Salamanca, Salamanca, Spain. [13]Department of Internal Medicine, University Hospital of Salamanca-IBSAL, Salamanca, Spain; Department of Medicine, University of Salamanca, Salamanca, Spain. [14]Department of Physical Performance, Norwegian School of Sport Sciences, Oslo, Norway.
*Corresponding author. Email: gsabio@cnio.es (G.S.); amorac@cnio.es (A.M.); cintia.folgueira@cnic.es (C.F.)
†These authors contributed equally to this work.

could be activated to promote spontaneous exercise in healthy individuals and patients with medical conditions.

RESULTS

Exercise induces activation of p38α in human muscle

The p38 pathway has been recognized as a crucial player in exercise-induced skeletal muscle adaptation. Notably, studies with transgenic and knockout (KO) mice have demonstrated that this pathway enhanced mitochondrial biogenesis, underscoring the importance of p38 in endurance exercise-induced muscle adaptation (*11*). Building on these findings, we sought to investigate the activation of p38α in human muscle after exercise. For this purpose, volunteers underwent an incremental exercise test on a cycle ergometer, and muscle biopsies were obtained from the vastus lateralis of one thigh before, immediately after, and 10 s after a 30-s maximal sprint (Wingate test). We found that exercise induces p38α activation in human muscle (Fig. 1A).

Mice deficient for p38α in striated muscle exhibit improved metabolism

To investigate the relevance of the p38 pathway in regulating muscle adaptations during exercise and its potential implications for human health, we generated conditional KO mice lacking p38α in striated muscle by expressing Cre recombinase under the muscle creatine kinase (MCK) promoter. Immunoblot images confirmed the absence of p38α in skeletal muscles (quadriceps, gastrocnemius, soleus, and extensor digitorum longus) and hearts of p38α$^{MCK\text{-}KO}$ mice, while no changes in p38α levels were observed in other tissues (fig. S1A).

We found that p38α$^{MCK\text{-}KO}$ mice had lower body weight than control mice when fed a normal chow diet (ND) (Fig. 1B and fig. S1B). Moreover, p38α$^{MCK\text{-}KO}$ mice displayed lower blood glucose levels in both fasted and fed states, along with improved glucose tolerance (Fig. 1, C and D).

Metabolic cages did not show changes in locomotor activity, energy expenditure, or respiratory quotient (RQ) compared to control mice (fig. S1, C to E) or anxiety-related behavior (which correspond with longer time spent on the periphery during the open field test) (fig. S2, A to E). However, p38α$^{MCK\text{-}KO}$ mice displayed improved fine motor coordination and balance, as evidenced by fewer slips and increased time on the beam in the balance beam assay (fig. S2, F to I). To gain a more comprehensive understanding of the mice's activity patterns comparable to human leisure time physical activity, we evaluated wheel engagement within the metabolic cages. This allowed us to measure both distance run and speed. Our findings revealed that p38α$^{MCK\text{-}KO}$ mice exhibit enhanced and faster running behavior (Fig. 1, E and F). In addition, no differences were observed in body temperature, interscapular temperature, or rectal temperature after cold exposure (fig. S2, J to L). These findings suggest that muscle-specific p38α deficiency contributes to improved metabolic outcomes.

p38α$^{MCK\text{-}KO}$ mice are protected against diet-induced obesity, diabetes, and liver steatosis

The lower body weight observed in ND-fed mice prompted us to investigate whether lack of p38α in striated muscle also conferred protection against obesity induced by a high-fat diet (HFD). HFD-fed p38α$^{MCK\text{-}KO}$ mice exhibited lower body-weight gain and weighed less than their control counterparts primarily due to a reduction in the weight of adipose depots (Fig. 2, A and B, and fig. S3A), indicating that muscle-specific p38α deficiency offers protection against HFD-induced obesity. HFD-fed p38α$^{MCK\text{-}KO}$ mice displayed higher locomotor activity (Fig. 2C) with more movement and total distance and showed no anxiety-like behavior, demonstrated by their lack of preference for the periphery in the open field (fig. S3, B to F). In concordance with this increased activity, they presented higher energy expenditure without affecting RQ or temperature (body or interscapular) (Fig. 2D and fig. S3, G to I). These findings support the notion that muscle-specific p38α deficiency contributes to increase the spontaneous locomotor activity and plays a role in the regulation of energy balance during HFD. We ruled out the possibility that the increased locomotor activity observed in these mice was due to protection against heart damage following the HFD, as they exhibited a reduction in p38α in the heart. Echocardiography analysis revealed no differences in heart function or structure, as measured by ejection fraction or fractional shortening, between genotypes (fig. S4, A to J).

HFD feeding can lead to hyperglycemia and hyperinsulinemia in mice, increasing the risk of insulin resistance and diabetes (*12*). The reduced fat accumulation in p38α$^{MCK\text{-}KO}$ mice led us to examine whether they were also protected against HFD-induced glucose intolerance. Analysis of plasma samples indicated that p38α$^{MCK\text{-}KO}$ mice had less severe HFD-induced hyperglycemia and hyperinsulinemia than wild-type (WT) mice (Fig. 2, E and F), as well as a lower homeostatic model assessment of insulin resistance (HOMA-IR) index, indicating lower insulin resistance (Fig. 2G). Furthermore, HFD-fed p38α$^{MCK\text{-}KO}$ mice exhibited enhanced glucose tolerance even when administered the same amount of glucose regardless of their weight (Fig. 2H and fig. S5A), correlating with higher glucose-induced insulin release (Fig. 2I). Higher insulin sensitivity in p38α$^{MCK\text{-}KO}$ mice was confirmed by insulin tolerance test (ITT; Fig. 2J). Immunoblot analysis of Akt phosphorylation, an index of insulin resistance (*12*), showed a higher insulin-induced Akt phosphorylation in the liver and skeletal muscle in p38α$^{MCK\text{-}KO}$ mice than that in control mice, indicating protection against insulin resistance in these organs in the KO mice (fig. S5, B to E). Hematoxylin and eosin (H&E) and Oil Red histological analysis of liver samples revealed a lower grade of hepatic steatosis in HFD-fed p38α$^{MCK\text{-}KO}$ mice than that in control mice (Fig. 2, K and L).

These results suggest that, in addition to protect against diet-induced obesity, the absence of p38α in muscle also protects against HFD-induced diabetes and hepatic steatosis.

p38α-deficient muscles hyperactivate p38γ and its upstream kinases

The observed changes in metabolism within skeletal muscle prompted us to investigate into the activation of p38γ, a key regulator identified in driving endurance exercise-induced metabolic adaptation in skeletal muscle (*11*). Western blot analysis revealed activation of p38γ in different skeletal muscles from HFD-fed p38α$^{MCK\text{-}KO}$ mice. This increase was not accompanied by changes in the total content of p38γ mRNA or protein (Fig. 3A and fig. S6, A to D). As expected, the specific p38α/β substrate mitogen-activated protein kinase (MAPK)–activated protein kinase 2 (MK2) (*13*) and the MK2 substrate, Hsp27, were not phosphorylated in HFD-fed p38α$^{MCK\text{-}KO}$ mice (fig. S6E), suggesting that p38α loss was not compensated by p38β kinase activity. Moreover, in line with the p38γ activation,

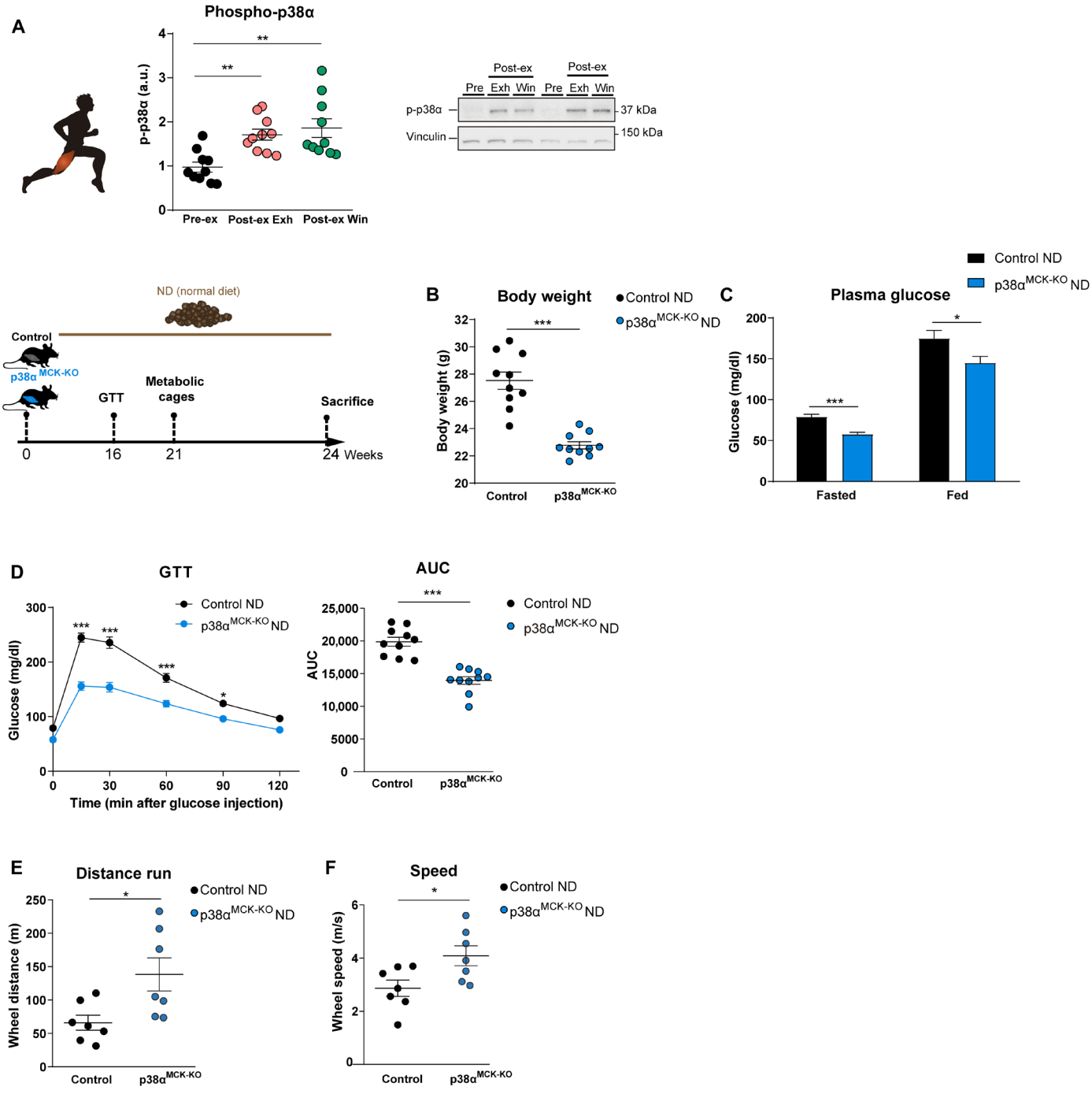

Fig. 1. Lack of p38α in striated muscle decreases body weight, improves glucose homeostasis, and exhibits enhanced and faster running behavior in mice fed an ND. (**A**) Representative Western blot of human muscle samples from two individuals before exercise (Pre) and immediately after exercise (Post) {at the end of the incremental test to exhaustion [post exhaustion test (Exh)] and post Wingate test (Win)} was examined with antibody against phospho-p38. Quantifications are shown. Vinculin protein expression was monitored as a loading control. Data are normalized to pre-exercise levels and shown as means ± SEM; $*P < 0.05$ and $**P < 0.01$. Student's *t* test; $n = 10$. a.u., arbitrary units. (**B** to **F**) Eight-week-old p38α^{MCK-KO} and control mice were fed a normal chow diet (ND). (B) Body weight; (C) fasting and fed plasma glucose levels at 16 weeks old; (D) glucose tolerance test (GTT) and area under the curve (AUC). Mice fasted overnight were injected intraperitoneally with glucose (1 g/kg) and blood glucose concentration was measured at the indicated time points. (E) Distance run and (F) speed during 24-hour period measured in metabolic cages with wheels. Data are shown as means ± SEM; $*P < 0.05$ and $***P < 0.001$; Student's *t* test (B to F); two-way analysis of variance (ANOVA) coupled to Bonferroni's multiple comparisons test (D); $n = 7$ to 13.

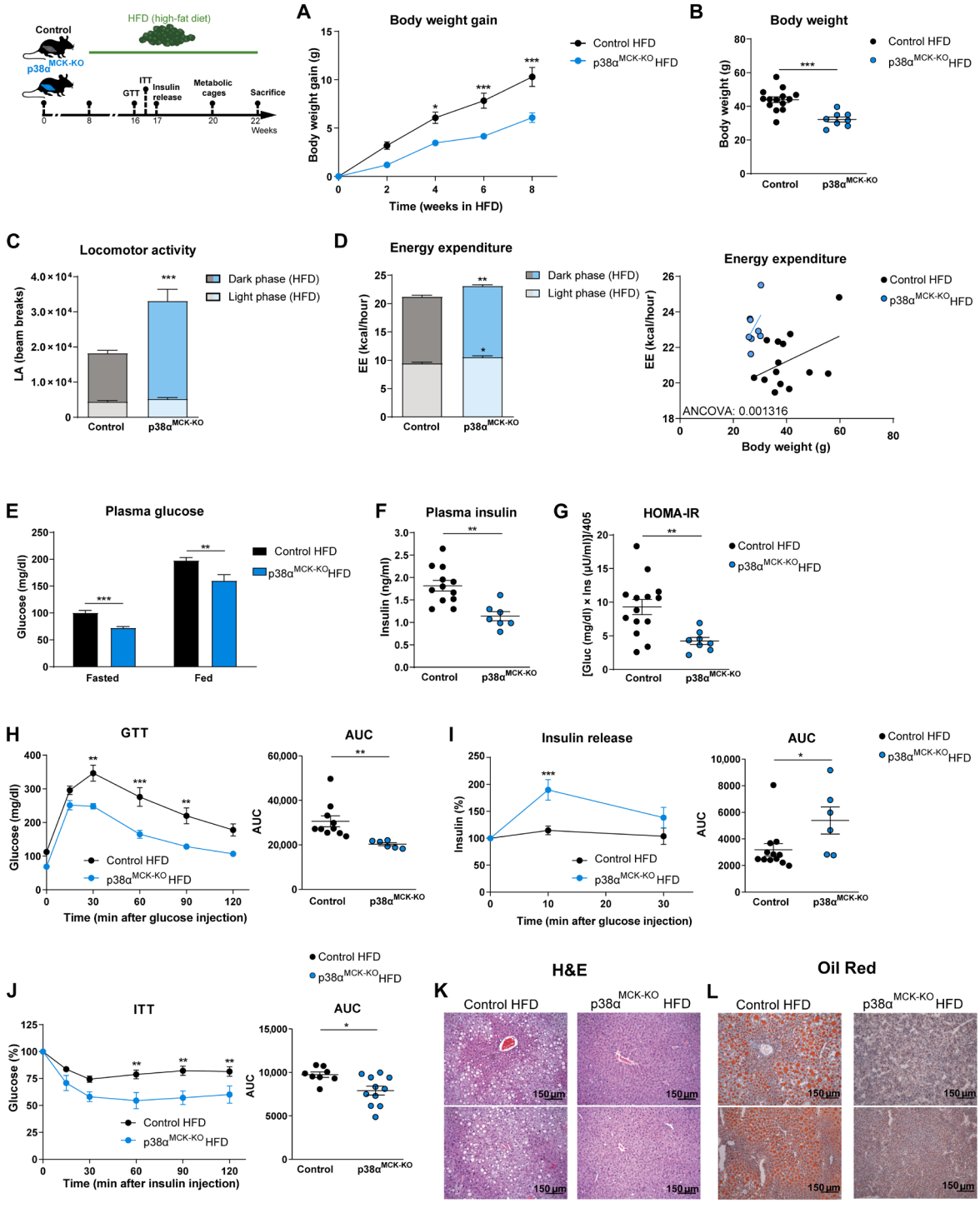

Fig. 2. Lack of p38α in striated muscle increases voluntary locomotor activity, protects against HFD-induced obesity, improves glucose metabolism, and reduces hepatic steatosis. p38α^{MCK-KO} and control mice were fed HFD, and body weight was monitored for 8 weeks. (**A**) Body weight gain measured at the indicated times during HFD treatment. (**B**) Body weight measured at sacrifice. (**C**) Locomotor activity (LA) during a 48-hour period after HFD. (**D**) Energy expenditure (EE) and analysis of covariance (ANCOVA). (**E**) Fasting and fed plasma glucose levels. (**F**) Fasting plasma insulin levels. (**G**) Insulin resistance rate calculated as homeostasis model assessment of insulin resistance (HOMA-IR) ratio. (**H**) GTT and AUC. Mice fasted overnight were injected intraperitoneally with glucose (1 g/kg). (**I**) Insulin release assay and AUC. Mice fasted overnight were injected intraperitoneally with glucose (2 g/kg), and insulin levels were measured at the indicated points. (**J**) Insulin tolerance test (ITT) and AUC. Mice fed ad libitum were injected intraperitoneally with insulin (0.75 U/kg). Blood glucose concentration was measured at the indicated points in GTT and ITT. Data are shown as means ± SEM; *$P < 0.05$, **$P < 0.01$, and ***$P < 0.001$; two-way ANOVA coupled to Bonferroni's multiple comparisons test (A and H to J); Student's *t* test [with Welch's correction for LA-dark phase, for glucose (fasted) and HOMA-IR] (B to J); $n = 6$ to 14. Gluc, glucose; Ins, insulin. (**K** and **L**) p38α^{MCK-KO} and control mice were fed an HFD, fasted overnight, and euthanized. (K) Representative H&E– and (L) Oil Red O–stained liver sections are presented. Scale bars, 150 μm. $n = 5$.

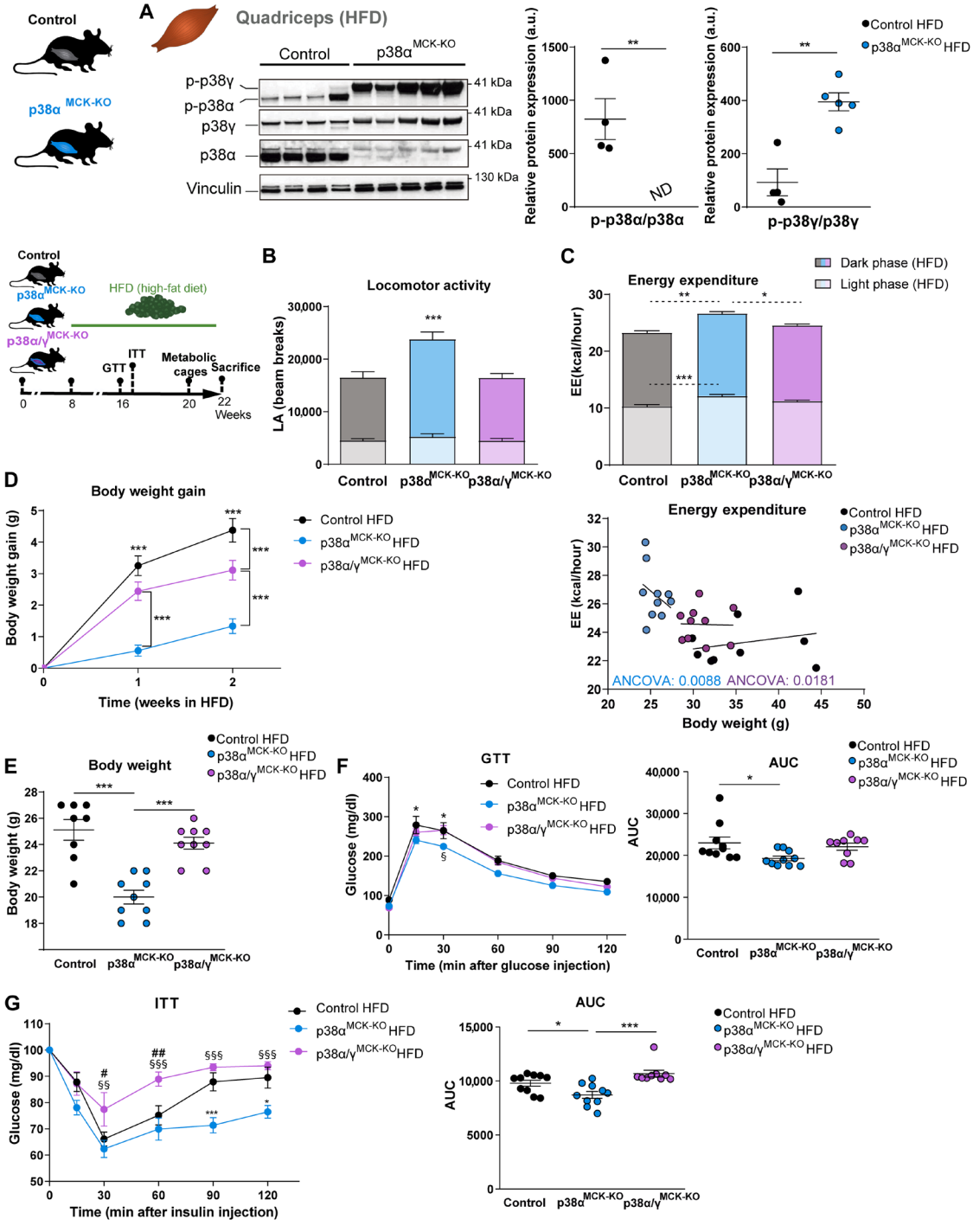

Fig. 3. Lack of p38γ in p38α^{MCK-KO} mice loses their protection against HFD-induced obesity and diabetes. Eight-week-old p38α^{MCK-KO} and control mice were fed an HFD, fasted overnight, and euthanized. (**A**) Extracts prepared from quadriceps were examined by immunoblot analysis with antibodies against phospho (p)–p38 and total protein levels. Quantifications are shown. Vinculin protein expression was monitored as a loading control. Student's *t* test; $n = 4$ to 5. (**B** and **C**) p38α/γ^{MCK-KO}, p38α^{MCK-KO}, and control mice were fed an HFD, and metabolic parameters were assayed. (B) LA and (C) EE and ANCOVA. Data are shown as means ± SEM; $^{*}P < 0.05$, $^{**}P < 0.01$, and $^{***}P < 0.001$; one-way ANOVA coupled to Bonferroni's multiple comparisons test; $n = 9$ to 10. * Symbols indicate differences between p38α^{MCK-KO} and control mice unless otherwise indicated. (**D** and **E**) p38α/γ^{MCK-KO}, p38α^{MCK-KO}, and control mice were fed HFD, and body weight was monitored for 2 weeks. (D) Body weight gain measured at the indicated times during HFD treatment. (E) Body weight measured during HFD feeding. Data are shown as means ± SEM; $^{***}P < 0.001$; one-way (E) or two-way ANOVA (D) coupled to Bonferroni's multiple comparisons test; $n = 8$ to 9. * Symbols indicate differences between p38α^{MCK-KO} and control mice unless otherwise indicated. (**F** and **G**) p38α/γ^{MCK-KO}, p38α^{MCK-KO}, and control mice were fed a HFD for 3 weeks. (F) GTT and AUC. (G) ITT and AUC. Data are shown as means ± SEM; *, #, or §$P < 0.05$; ## or §§$P < 0.01$; *** or §§§$P < 0.001$; two-way ANOVA coupled to Bonferroni's multiple comparisons test; $n = 9$ to 10. * Symbols depict significant differences between p38α^{MCK-KO} and control mice; # symbols indicate significant differences between p38α/γ^{MCK-KO} and control mice; and § symbols depict significant differences between p38α/γ^{MCK-KO} and p38α^{MCK-KO} mice.

p38α deficiency triggered activation of the two main upstream MAPK kinases (MAP2K) in the p38 signaling pathway, MKK3 and MKK6, linked to increased MKK3 and MKK6 mRNA and total protein expression (fig. S6, E to G). These findings suggest that the absence of p38α in muscle leads to the activation of p38γ and its upstream kinases, providing valuable insights into the molecular basis of the observed metabolic pathway changes in p38α-deficient skeletal muscle.

p38γ activation in p38α-deficient muscle mediates protection against obesity

Given the implication of p38γ in obesity comorbidities (*14*, *15*), we investigated the influence of p38γ phosphorylation on the phenotype of mice lacking p38α in striated muscle. To address this, we generated mice with striated muscle deletion of both p38α and p38γ (p38α/γ$^{MCK\text{-}KO}$). Upon HFD feeding, we observed that the lack of p38γ reversed the protective phenotype associated with striated-muscle p38α deficiency, because p38α/γ$^{MCK\text{-}KO}$ mice display lower locomotor activity linked to the reduced energy expenditure that was associated with higher body weight and body weight gain compared to p38α$^{MCK\text{-}KO}$ mice (Fig. 3, B to E). No discernible differences between genotypes in RQ or temperature (body or interscapular) were observed (fig. S7, A to C). These results highlight the crucial role of p38γ activation in mediating the protective effects against obesity observed in p38α$^{MCK\text{-}KO}$ mice. In agreement with the loss of obesity protection, p38α/γ$^{MCK\text{-}KO}$ mice exhibited impaired glucose tolerance and insulin sensitivity (Fig. 3, F and G), similar to the values observed in control mice. These results provide compelling evidence that p38γ activation in p38α$^{MCK\text{-}KO}$ skeletal muscle is instrumental in conferring protection against obesity and diet-induced diabetes.

p38γ activation increases voluntary physical activity

Our data suggest that activating p38γ in muscle enhances locomotor activity. To test this hypothesis, we overexpressed active p38γ in muscle using an adeno-associated virus (AAV-sk-cm4-cherry-p38γ*) (Fig. 4A). Metabolic cages demonstrated that muscle expression of active p38γ increased locomotor activity (Fig. 4B). In addition, mice overexpressing active p38γ in muscle exhibit increased and quicker voluntary wheel running, suggesting that p38γ in muscle tissue plays a role in incentivizing voluntary physical activity (Fig. 4, C and D). This increase of locomotor activity resulted in reduced weight gain (Fig. 4E). To gain insights into how muscle p38γ might influence exercise performance, we conducted a treadmill exhaustion test. While the absence of muscle p38α resulted in a slight increase in maximal velocity and distance, the expression of active p38γ in muscle increased both maximal velocity and distance, suggesting that the activation of p38γ improves exercise performance (Fig. 4, F and G). Maximum speed, work performed, and distance to exhaustion were all higher in p38γ* animals, demonstrating durable and substantially increased levels of physical endurance (Fig. 4G). Furthermore, our analysis revealed no differences in the open field test between mice overexpressing p38γ* in muscle and control group, indicating that the observed increase in locomotor activity is not due to altered exploratory behavior or anxiety levels (fig. S7, D to H).

Activation of p38γ induces the secretion of IL-15, which, in turn, increases locomotor activity

Exercise can stimulate the release of myokines in skeletal muscle, potentially contributing to metabolic improvements. To evaluate whether lack of muscle p38α can affect myokine production, improving metabolism, we performed transcriptomic analysis of p38α$^{MCK\text{-}KO}$ muscle. Through RNA sequencing (RNA-seq)–based transcriptomic analysis of control, p38α$^{MCK\text{-}KO}$ and p38α/γ$^{MCK\text{-}KO}$ muscles, combined with secretome screening for genes encoding secreted proteins, we identified 15 differentially expressed genes (DEGs) in p38α$^{MCK\text{-}KO}$ mice likely to encode secreted proteins, including IL-15, a well-known myokine linked to locomotor activity control (*16*–*18*). The analysis revealed increased IL-15 expression in p38α$^{MCK\text{-}KO}$ muscle but not in p38α/γ$^{MCK\text{-}KO}$ muscles, confirmed by quantitative polymerase chain reaction (qPCR) (Fig. 5, A to D). Furthermore, we corroborate that p38α$^{MCK\text{-}KO}$ mice display higher plasma IL-15 concentrations than control mice (Fig. 5E). In addition, both muscle and plasma IL-15 levels increase with the overexpression of p38γ in muscle (fig. S7, J and K). IL-15 production involves diverse cell types with evidence pointing to its generation by not only conventional immune cells but also other types of cells as myocytes. To evaluate whether myocytes can produce this cytokine, we analyze single-cell public datasets (*19*) (https://rstudio-connect.hpc.mssm.edu/muscle-multiome/). This reveals that myogenic cells, derived from muscle progenitors, exhibit elevated IL-15 levels compared to mesenchymal or neuronal cells (fig. S8A). In addition, we found that muscle fibers can produce IL-15 (fig. S8B). These results suggest that, in the muscles of p38α$^{MCK\text{-}KO}$ mice, p38γ activation induced IL-15 release, contributing to their higher spontaneous locomotor activity.

To confirm that IL-15 increases voluntary physical activity, we treat animals with IL-15 intravenously. Metabolic cage analysis reveals that IL-15 increases both locomotor activity and energy expenditure (Fig. 5, F and G). Released by skeletal muscle, IL-15 can influence brain function (*20*) and has also been associated to lower anxiety-related behaviors (*21*, *22*). Compared with the other genotypes, p38α$^{MCK\text{-}KO}$ mice also showed a tendency toward lower depression-like behavior (less immobility) in the tail suspension test (Fig. 5H).

IL-15 signaling in the brain primary and secondary motor cortices (M1 and M2) controls movement (*23*). Therefore, we investigated whether the elevated muscle IL-15 in p38α$^{MCK\text{-}KO}$ mice affects motor cortex signaling. We observed higher phosphorylation of extracellular signal–regulated kinase (ERK), signal transducer and activator of transcription 3 (STAT3), and STAT5 in these brain areas of p38α$^{MCK\text{-}KO}$ mice (Fig. 5I), suggesting that higher IL-15 signaling in the motor cortex might contribute to the elevated locomotor activity in p38α$^{MCK\text{-}KO}$ mice. To test this hypothesis, we suppressed IL-15 signaling in M1 by using a stereotaxic procedure to inject short hairpin RNA (shRNA) against the α subunit of the IL-15 receptor (IL-15Rα; shIL-15Rα) (Fig. 5J). p38α$^{MCK\text{-}KO}$ mice with reduced motor cortex IL-15Rα expression exhibited lower locomotor activity (Fig. 5K), glucose intolerance, and body weight (Fig. 5, L and M, and fig. S8C) than p38α$^{MCK\text{-}KO}$ mice injected with control shRNA (shScramble). Moreover, p38α$^{MCK\text{-}KO}$ mice treated with shIL-15Rα displayed a higher depression-like behavior in the tail suspension test to those treated with control shRNA (Fig. 5N).

Muscle p38γ activation upon exercise stimulates IL-15 secretion

Our results suggest that p38γ activation in muscle plays a role in promoting IL-15 production, thereby enhancing voluntary physical activity and contributing to improved health. To further understand the physiological relevance of this pathway, we investigated the response of p38γ activation during exercise. WT mice were subjected

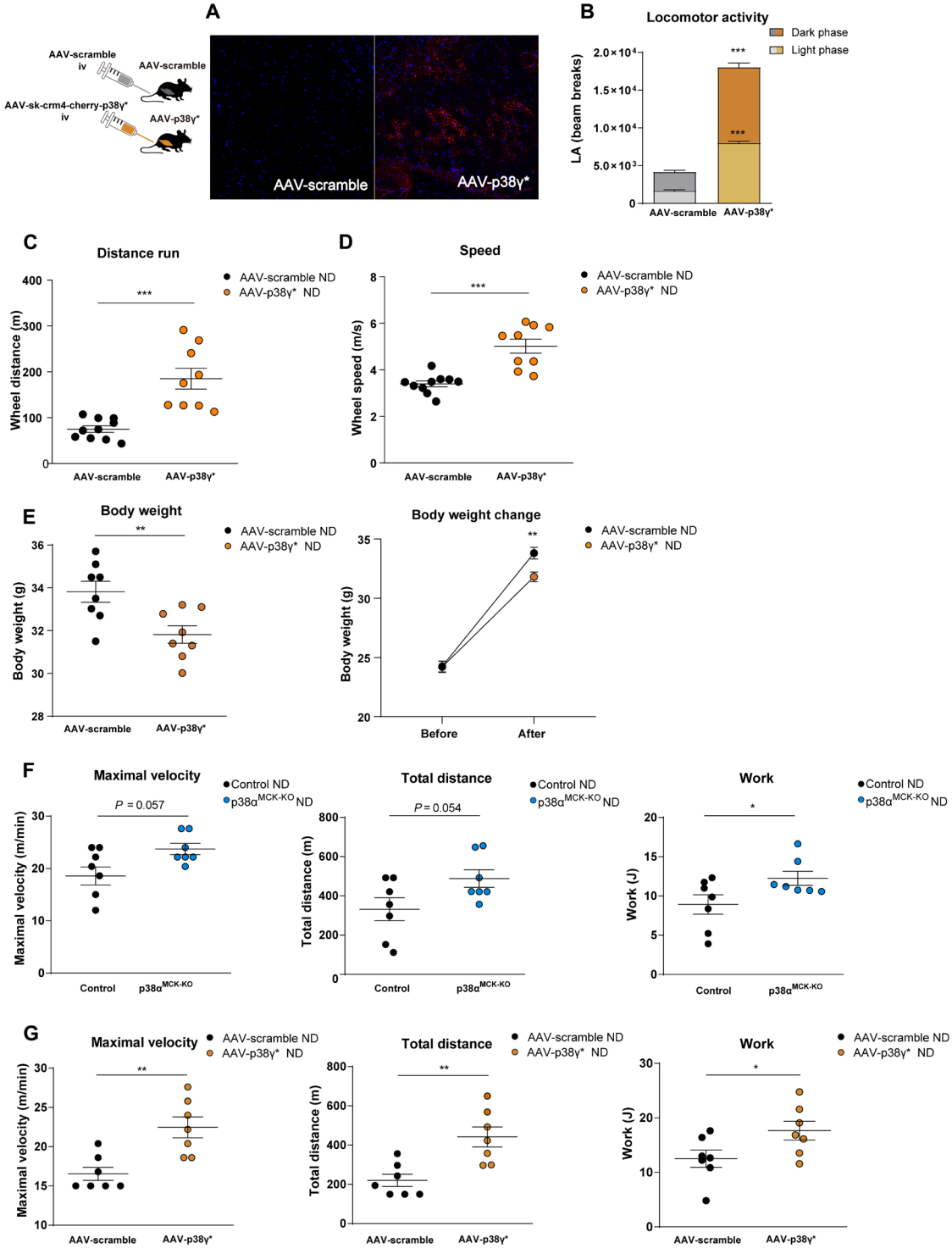

Fig. 4. p38γ activation increase LA. Eight-week-old WT mice fed an ND were injected intravenously (iv) with 5×10^{11} per mice AAV-scramble or AAV-sk-cm4-cherry-p38γ* (active p38γ). (**A**) Representative anti-cherry immunohistochemistry muscle sections are presented at ×20 magnification. (**B**) LA, (**C**) wheel distance run, (**D**) wheel speed in metabolic cages, and (**E**) body weight change 4 weeks after AAV-scramble or AAV-sk-cm4-cherry-p38γ* intravenous injection. (**F** and **G**) Measurement of exercise capacity using a graded exercise treadmill, and mice were run to exhaustion. (F) Maximal velocity, total distance, work, and power were evaluated in $p38\alpha^{MCK\text{-}KO}$ and control mice and (G) in WT mice 4 weeks after AAV-scramble or AAV-sk-cm4-cherry-p38γ* intravenous injection. Data are shown as means ± SEM; $^{*}P < 0.05$, $^{**}P < 0.01$, and $^{***}P < 0.001$. Student's *t* test (B to G); $n = 7$ to 10.

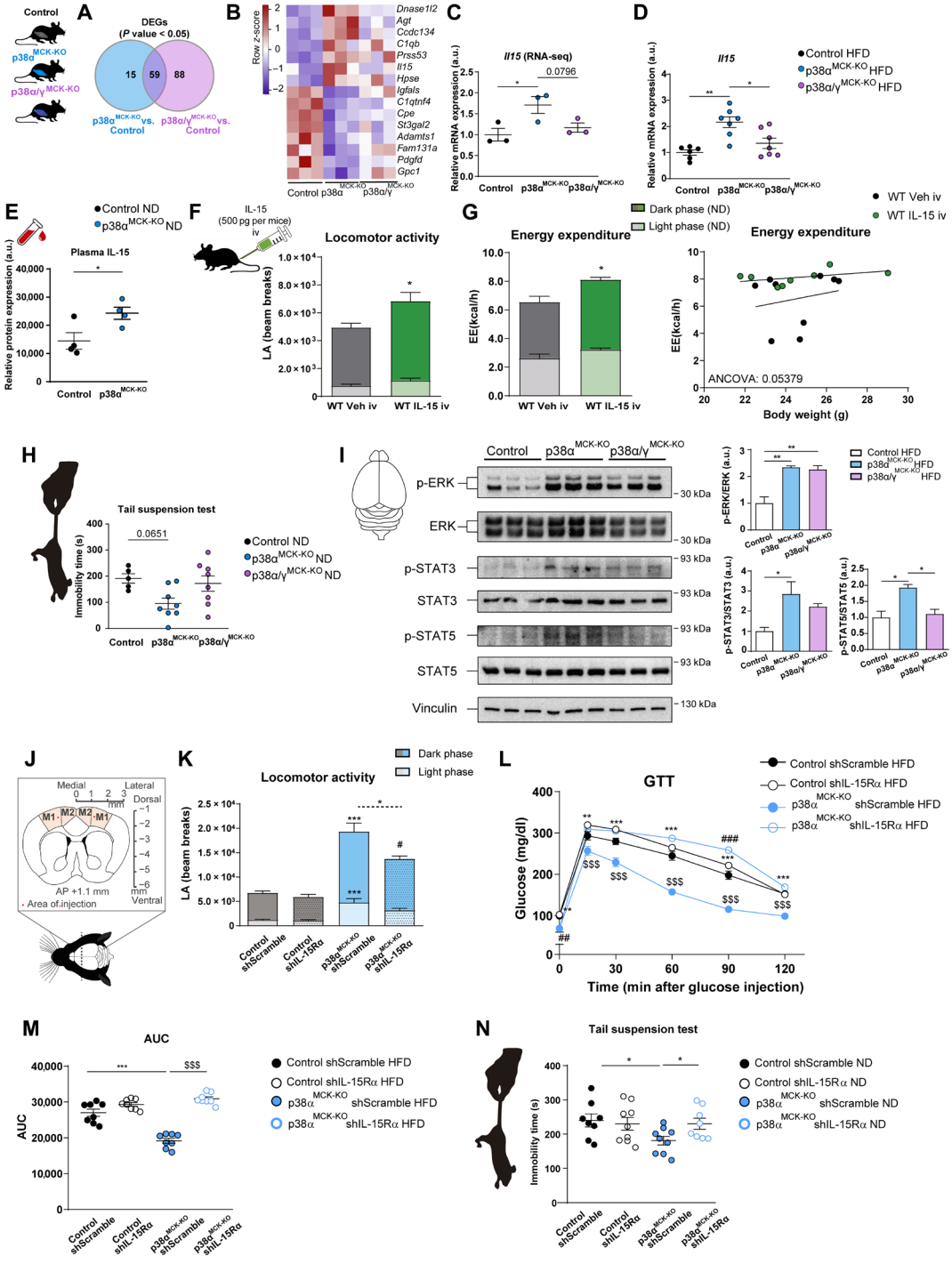

Fig. 5. p38α^{MCK-KO} mice have higher muscle IL-15 expression and increased plasma IL-15 levels following exercise controlled by the motor cortex. (**A** to **C**) RNA-seq analysis with gastrocnemius samples from HFD-fed p38α^{MCK-KO}, p38α/γ^{MCK-KO}, and control mice, fasted overnight. (A) Venn diagram illustrating differentially expressed genes (DEGs) for secreted proteins comparing p38α^{MCK-KO} or p38α/γ^{MCK-KO} mice with controls, (B) heatmap, (C) *Il-15* mRNA expression in RNA-seq. (**D**) *Il-15* measure by qRT-PCR normalized to *Rps18* mRNA. Data are normalized to control mice (**E**) IL-15 levels of mice subjected to treadmill exercise for 30 min. (**F** and **G**) Eight-week-old WT mice fed an ND were injected iv with IL-15 (500 pg per mice). (F) LA and (G) EE and ANCOVA 48 hours after injection. (**H**) Tail suspension test performed in 18- to 23-week-old mice fed a ND. (**I**) Extracts prepared from the motor cortex were examined by immunoblot analysis with indicated antibodies. Data are normalized to control mice. (**J** to **N**) Eight- to 11-week-old mice were injected in the motor cortex with an shRNA targeting IL-15Rα (shIL-15Rα) or a control sequence (shScramble) by stereotaxic surgery. (J) Schematic representation of the brain area targeted during the surgical procedure. (K) LA during a 48-hour period 4 weeks after stereotaxic injection. (L and M) Four weeks after stereotaxic injection p38α^{MCK-KO}, and control mice were placed on an HFD and GTT and AUC were measured. Mice fasted overnight were injected intraperitoneally with glucose (1 g/kg). (N) Tail suspension test was performed. Data are shown as means ± SEM; (A to D, H, and I) one-way ANOVA coupled to Bonferroni's multiple comparisons test or Student's *t* test (E and G); *, $, or #*P* < 0.05; **, $$, or ##*P* < 0.01; ***, $$$, or ###*P* < 0.001.

to treadmill exercise and evaluated p38γ activation in the muscle after 30 min of exercise. Our findings revealed that acute exercise induced increased levels of p38γ activation in the muscle (Fig. 6A). This correlates with an increase of IL-15 in plasma, which aligns with its role in regulating IL-15 expression (Fig. 6B). These results further support the notion that p38γ is involved in the regulation of IL-15 production during exercise and highlights the potential relevance of this pathway in modulating physical activity and health benefits.

p38α and p38γ kinases are differentially regulated after training

Our findings indicate that both p38α and p38γ are activated after exercise but play opposing roles in regulating voluntary physical activity. p38γ promotes IL-15 production, enhancing voluntary physical activity, whereas p38α appears to inhibit p38γ activation, acting as a brake. This regulatory mechanism might ensure a balanced response to exercise, controlling its duration and intensity to prevent overexertion. To assess whether training changes the relative activation of these kinases, we evaluated p38α and p38γ activation in both trained and non-trained animals. After 5 weeks of aerobic training, we observed higher expression and activation of p38γ, while p38α activation remained reduced (Fig. 6, C and D). This suggests a shift in the balance between these regulators during training, where increased p38γ activation may contribute to enhanced exercise tolerance.

The p38γ/IL-15 axis is activated in human muscle after exercise

To confirm the relevance of the p38γ/IL-15 axis in human muscle, we analyzed muscle biopsies from individuals who underwent incremental exercise to exhaustion (*24*). Consistent with our earlier observations in mice, the phosphorylation of p38γ and the expression of IL-15 were found to be increased in human muscle after exercise (Fig. 6E). Furthermore, we observed a corresponding increase in plasma IL-15 levels following exercise (Fig. 6F). These findings reinforce the clinical importance of the p38γ/IL-15 axis, suggesting that this signaling pathway plays a crucial role in regulating physical activity in both mice and humans.

Using a cohort consisting of both healthy participants and individuals with obesity (Table 1), we investigated plasma IL-15 levels. Unexpectedly, our analysis revealed reduced blood levels of this myokine in individuals with obesity (Fig. 6G), further suggesting its potential involvement in obesity and related metabolic disorders. Together, these findings emphasize the crucial role of p38γ activation in muscle and its connection to IL-15 production, both during acute exercise and in response to incremental exercise in human subjects. This pathway's clinical relevance is further supported by its association with reduced plasma IL-15 levels in patients with obesity, suggesting its potential as a target for interventions aimed at addressing obesity and related metabolic disorders.

DISCUSSION

Exercise has been recognized as a beneficial strategy for combating obesity and improving metabolic homeostasis, partly attributed to the secretion of myokines from skeletal muscle. In our study, we discover that p38γ is activated in human muscle after exercise, suggesting its potential role in promoting metabolic health. Our findings demonstrate that p38γ expressed in skeletal muscle enhances the production and secretion of IL-15 by the muscle, leading to increased activation of the motor cortex and subsequent elevation in spontaneous locomotor activity. This heightened locomotor activity results in higher energy expenditure, offering protection against obesity, diabetes, and liver steatosis.

IL-15 appears to be a key player in driving the high locomotor activity observed in p38α^{MCK-KO} mice. IL-15 is among several factors secreted by skeletal muscle that are elevated following exercise in mice and humans (*7*). However, the regulation of muscle-derived IL-15 and its physiological consequences have remained unclear. While some studies have reported elevated IL-15 levels in humans after exercise (*16*, *25*), others have not observed these changes (*26*). In our study, following endurance exercise, we observed a tendency for increased IL-15 levels in the blood and the use of occlusion intensified this increase. However, we cannot exclude the possibility that secretion of IL-15 is very limited in the time, and, therefore, occlusion might have allowed for the accumulation of IL-15 in muscle (or interstitial space) and facilitated the detection of IL-15 increases in muscle and blood immediately after exercise. Previous research has described a relatively transient increase in IL-15 in circulation immediately following exercise (*16*, *25*), suggesting the importance of timing in blood sampling to detect the exercise response. Moreover, an immediate change in circulating IL-15 levels implies the presence of a pool of readily secretable IL-15 that may not necessarily depend on transcriptional changes in IL-15 mRNA (*16*).

Our results suggest that higher muscle IL-15 expression facilitates its secretion after exercise. Higher exercise-induced plasma IL-15 appears to signal the cerebral motor cortex to enhance voluntary locomotor activity and reduce depression-like behavior, a conclusion supported by the reduced locomotor activity in p38α^{MCK-KO} mice upon suppression of motor cortex expression of IL-15Rα. Although we cannot pinpoint muscle-derived IL-15 as the exclusive source, the link between exercise and increased IL-15 action is evident in our findings, reinforcing the importance of IL-15 signaling in this area for the control of voluntary movements.

The regulation of muscle-derived IL-15 and its physiological consequences remain unclear, although IL-15 has been linked to reductions in adiposity and protection against type 2 diabetes and fatty liver disease (*27*–*29*). Moreover, there is also controversy about the role of IL-15 signaling in the control of locomotor activity, with IL-15 reported to enhance (*16*) or to decrease locomotor activity (*17*, *18*). This controversy also applies to the role of IL-15 in the modulation of anxiety and depression (*21*, *22*, *30*). Our results indicate that IL-15 signaling in the motor cortex contributes to the increased locomotor activity, establishing an important cross-talk between the muscle and the brain.

In addition to its role in activating p38γ and promoting IL-15 production, our data reveal that p38α exerts a negative regulation over p38γ. This negative feedback of p38α on p38γ has been reported in previous studies (*31*, *32*), further highlighting the complexity of the p38 family and the need to comprehensively understand the distinct functions of its different members. Our results suggest that p38α activation serves to block the activation of p38γ, which, in turn, regulates IL-15 and the reward or interest associated with exercise. We have observed that exercise activates both p38α and p38γ in muscle. These kinases exert opposing effects: While p38γ enhances voluntary physical activity, p38α refrain it by inhibiting p38γ activation and IL-15 production. This coordinated action might

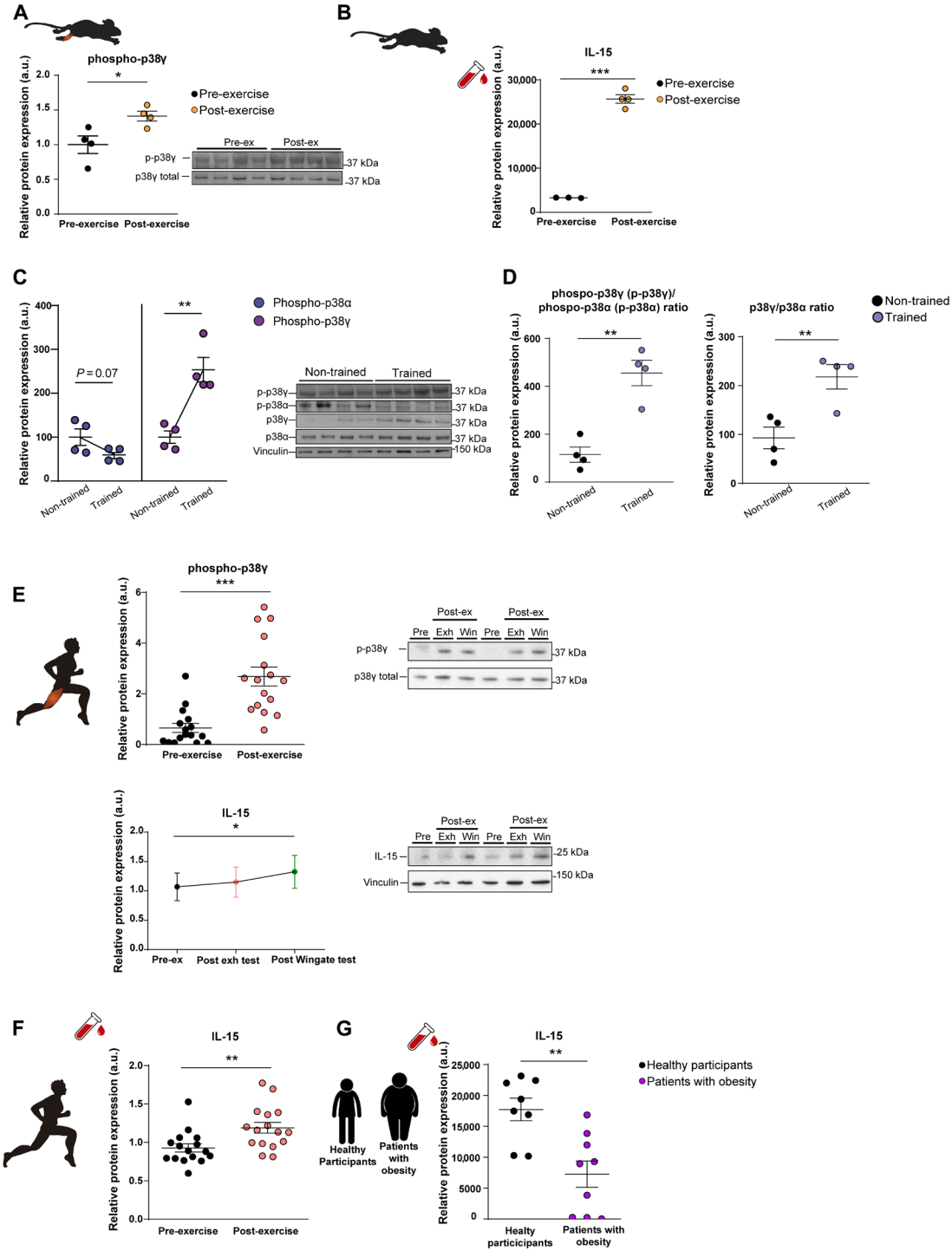

Fig. 6. Muscle p38γ activation upon exercise stimulates IL-15 secretion. (**A** and **B**) Eight-week-old control mice were subjected to treadmill exercise for 30 min, and (A) gastrocnemius and (B) blood samples were extracted after exercise. Immunoblot analysis and quantification of muscle phospho-p38γ, p38γ total, and circulating IL-15 levels immediately after exercise are shown. Data are shown as means ± SEM; $^{*}P < 0.05$, $^{**}P < 0.01$, and $^{***}P < 0.001$; Student's *t* test; $n = 4$. (**C** and **D**) Gastrocnemius samples were extracted from trained and non-trained mice. Immunoblot analysis and quantification of muscle phospho-p38γ (p-p38γ)/phospho-p38α (p-p38α) and phospho-p38γ (p-p38γ)/phospho-p38α (p-p38α) ratio and p38γ/p38α ratio. Vinculin protein expression was monitored as a loading control. Data are shown as means ± SEM; $^{**}P < 0.01$; Student's *t* test; $n = 4$. (**E**) Muscle human samples obtained before exercise, immediately after exercise (at the end of the incremental test to exhaustion (post exhaustion test) and post Wingate test) were examined by immunoblot analysis with antibodies against phospho-p38γ, p38γ total, and IL-15. Vinculin protein expression was monitored as a loading control. (**F**) Il-15 circulating levels were measured in human samples obtained before exercise and after exercise. Quantifications are shown. Data are normalized to pre-exercise levels and shown as means ± SEM; $^{*}P < 0.05$, $^{**}P < 0.01$, and $^{***}P < 0.001$. Student's *t* test; $n = 13$ to 16. (**G**) Circulating IL-15 expression in patient controls and patients with obesity. Data are shown as means ± SEM; $^{**}P < 0.01$. Student's *t* test; $n = 8$ to 9.

Table 1. Characteristics of obese patients and controls for human plasma samples. Variables are presented as mean (SD) or absolute frequency (percentage) and are compared by means of chi-square test. BMI, body mass index; AST, aspartate aminotransferase; ALT, alanine aminotransferase; LDL, low-density lipoprotein; HDL, high-density lipoprotein.

Variable	Patients with obesity ($n = 11$)	Patient controls ($n = 9$)	*P*
Age (years)	47.6 (11.60)	53.11 (16.16)	0.40
BMI (kg/m^2)	48.816 (8.527)	24.13 (2.27)	<0.0001
Body fat (%)	47.77 (4.26)	24.20 (3.76)	<0.0001
Fasting blood sugar (mM)	7.14 (4.18)	5.16 (0.57)	0.236
Insulin (pM)	807.013 (648.11)	114.27 (24.50)	0.021
HOMA-IR	8.16 (9.57)	0.742 (0.15)	0.082
AST (IU/liter)	28.3 (12.45)	36.57 (39.66)	0.542
ALT (IU/liter)	38.7 (16.47)	32 (23.62)	0.512
Total cholesterol (mM)	4.95 (1.27)	4.68 (1.28)	0.69
Triglycerides (mM)	1.92 (1.14)	1.26 (0.52)	0.184
LDL-cholesterol (mM)	2.77 (1.56)	2.98 (1.17)	0.786
HDL-cholesterol (mM)	1.01 (0.19)	1.12 (0.32)	0.446

ensure that exercise provides a rewarding experience and promotes further activity while also preventing exhaustion and overexertion by limiting excessive activity. Training shifts the balance between p38α and p38γ, favoring increased activation of p38γ, which may contribute to enhanced exercise tolerance. Previously, we have observed a similar coordinated action of the same both kinases to avoid loss of energy associated with excessive brown adipose tissue (BAT) thermogenesis (*31*). We believe that this illustrates a consistent pattern of control over energy balance and expenditure. Moreover, our experiments in mice demonstrate that deleting p38α in muscle tissue leads to an increase in voluntary physical activity compared to controls. Further experiments are needed to fully understand how this regulatory pathway operates in humans, particularly during training and in conditions such as obesity. Our results suggest that IL-15 increases spontaneous physical activity, which, in humans, is equivalent to leisure time physical activity. To ascertain whether repeated exercise-induced IL-15 increases could translate into enhanced exercise adherence in humans will require further experiments. Continued research in this area will provide valuable insights into the physiological mechanisms underlying exercise behavior and its modulation in various contexts.

The existence of these opposing regulatory mechanisms emphasizes the importance of elucidating the specific roles of individual family members to fully grasp their contributions to cellular processes and physiological outcomes. As we understand better the functions of the p38 family, we gain valuable insights that can improve the development of targeted therapeutic strategies for addressing various metabolic disorders and related health challenges.

This study identifies skeletal muscle p38γ as a central signaling hub involved in the amount of physical exercise undertaken by inducing IL-15 production. The presence of this pathway in humans offers a promising target for the development of therapeutic approaches to combat the obesity epidemic. Understanding the interplay between muscle and brain signaling pathways could open up avenues for interventions aimed at promoting physical activity and metabolic health.

MATERIALS AND METHODS

Exercise responses in humans: Study population

Seventeen young men volunteered to participate in this study [means ± SD; age, 22.5 ± 2.4 years; body mass, 72.7 ± 7.6 kg; height, 178 ± 8 cm; body fat, 18.6 ± 5.8%; body mass index (BMI), 23.1 ± 2.3 kg m^{-2}; and maximal oxygen consumption VO_2max, 47.9 ml kg^{-1} min^{-1}]. The inclusion criteria were (i) age between 18 and 35 years, < 30 kg m^{-2}; (ii) sex, male; (iii) normal resting 12-lead electrocardiogram; and (iv) having a physically active lifestyle exercising regularly two to four times a week, but without following a specific training program. The exclusion criteria were (i) any disease or allergy, (ii) any medical contraindication for exercise, (iii) smoking, and (iv) being under any medical treatment. The study was approved by the Ethical Committee of the University of Las Palmas de Gran Canaria and was carried out by the Declaration of Helsinki (CEIH-2015-03). All volunteers received written and oral information regarding the aims of the study and the associated risk and signed a written consent before starting the experiments. Subjects were requested to avoid drinking caffeine, taurine, or alcohol-containing beverages and not to exercise 24 hours before the experiments. Besides, they were asked to maintain their usual diet until the end of the study. Upon completion of the study, all participants received a small monetary compensation, which was approved by the ethical committee. The study was designed to determine the main signaling pathways activated by cellular stress during exercise and after exercise ischemia, using an experimental model previously characterized (*24*).

Exercise responses in humans: Pretest and familiarization

During the first visit to the laboratory, anthropometric measurements were taken, and their body composition was assessed using dual-energy x-ray absorptiometry (Lunar iDXA, GE Healthcare, Milwaukee, WI, USA) (*33*). After that, the volunteers visited the laboratory on at least three additional days for familiarization with experimental procedures by performing an incremental exercise to exhaustion and sprint exercise (30-s Wingate all-out test). This was

continued by three sessions to determine their (VO_2max); in one session, an incremental exercise to exhaustion was carried out as previously reported (*34*), and, during the other two sessions, they performed repeated supramaximal exercise bouts at 120% of VO_2max until exhaustion, interspaced with 20-s recovery periods, 1 day recovering with a free circulation and the other with total occlusion of the circulation (*34*). The exercise tests were carried out on a Lode ergometer (Groningen, The Netherlands), while subjects were requested to maintain a pedaling cadence close to 80 rpm (*33*, *34*). Exhaustion was defined by the subject stopping pedaling suddenly or by a drop in the pedaling cadence below 50 rpm despite strong verbal encouragement for 5 s. The highest 20-s averaged VO_2 value recorded during the incremental exercise to exhaustion or repeated supramaximal exercise bouts was taken as the VO_2max (*35*). Oxygen uptake was measured breath by breath using a metabolic cart (Vyntus, Jaeger-CareFusion, Höchberg, Germany) calibrated immediately before each test using high-grade certified gases provided by the manufacturer. The volume flow sensor was calibrated immediately before each test at low (0.2 liter/s) and high (2 liter/s) rates. The validity of this metabolic cart was established by a butane combustion test (*36*).

Exercise responses in humans: Main experiment

One week after the VO_2max assessment, volunteers reported to the laboratory at 07.00 hours, following a 12-hour overnight fast. Both femoral veins were catheterized under local anesthesia (2% lidocaine) before the exercise tests using the Seldinger technique as previously reported (*33*). After catheterization, a first basal muscle biopsy was obtained from the m. vastus lateralis of one of the two thighs, assigned randomly, using the Bergstrom's technique with suction, as previously reported (*24*). The needle was directed distally for the first biopsy, with 45° inclination (*37*) and the skin incision covered with a temporary dressing easy to remove at exhaustion. After that, a cuff (SCD10, Hokanson, Bellevue, WA, USA) connected to a rapid cuff inflator (Hokanson, E20 AG101) was placed around the thighs (chosen randomly), as close as possible to the inguinal crease, and a resting blood sample was obtained from one of the femoral veins. Then, the subjects sat on the cycle ergometer, and, after verification of proper readings, the incremental exercise test started with 3 min at 20 W, followed by 20-W increases every 3 min until the respiratory exchange ratio was ≥1.00. After that, the ergometer was unloaded while the subjects kept pedaling at 30 to 40 rpm for 2 min. Then, the exercise intensity was increased to the same reached at the end of the previous phase and increased by 15 W every minute until exhaustion. At this moment, the cuff was inflated instantaneously at 300 mmHg, and a second biopsy was obtained 20 s after exhaustion. For this second biopsy, the needle was introduced perpendicular to the thigh (*37*). Then, the subject rested quietly on the cycle ergometer and was prepared to perform a 30-s maximal sprint (Wingate test) with the ergometer set in isokinetic mode (80 rpm) exactly 60 s after exhaustion. During these 60 s, the cuff remained inflated, and the circulation occluded in the cuffed leg. At the start of the 30-s sprint, the cuff was instantaneously deflated and reinflated at 300 mmHg at the end of the 30-s sprint. Exactly 10 s after the sprint, a third muscle biopsy was obtained from the occluded leg. For this third biopsy, the needle was introduced with a 45° inclination and pointing proximally (*37*). Immediately after the biopsy, the incision was covered, and the subject moved carefully to a stretcher where he rested in the supine position with the circulation of leg biopsied fully occluded. Ninety seconds after the end of the exercise, the cuff was deflated, and, 30 s later, a bilateral blood sample was obtained simultaneously from both femoral veins. Thus, one leg that had an occluded circulation of 60 s after the incremental exercise and another lasting 90s after the sprint exercise and the contralateral leg with always with a free circulation. All biopsies were immediately frozen in liquid nitrogen and stored at −80°C. The blood samples (6 ml) were collected into vacutainer tubes with EDTA (BD Medical 368861 Vacutainer PET) and immediately centrifuged at 2000*g* at 4°C for 10 min. The plasma obtained was stored at −80°C.

Study patient controls and patients with obesity and sample collection

For the analysis of human levels of blood IL-15 in patient controls and patients with obesity, the study population included 19 patients (11 adult patients with BMI ≥ 35) and control subjects (n = 8, BMI ≤ 30). Baseline characteristics of these groups are listed in Table 1. Fasting blood samples were collected for IL-15 analysis. Blood was extracted using straight needles (21-gauge butterfly) and Vacuette Z Serum Sep Clot Activator tubes. After 30 min, these tubes were centrifuged at 1500 rpm for 10 min at room temperature to separate serum, which was divided into aliquots and stored at −80°C until further analysis. Patients were excluded if they had a history of alcohol use disorders or excessive alcohol consumption (>30 g/day in men and >20 g/day in women), had chronic hepatitis C or B, or if laboratory and/or histopathological data showed causes of liver disease other than metabolic associated fatty liver disease. The study was approved by the Ethics Committee of the University Hospital of Salamanca and the Instituto de Salud Carlos III (Código CEIm: PI 2020 12 653) with all subjects providing a written informed consent to fasting blood extraction.

Mouse model

Mice carrying the floxed p38α alleles (B6.129-*Mapk14*$^{tm2.1}$/N) were generated by Boehringer Ingelheim Pharmaceuticals and have been described previously (*38*). These mice were crossed with mice expressing Cre recombinase under the MCK promoter [FVB-Tg (*Ckmm-cre*)*5Khn*/N; control mice] to conditionally delete p38α from striated muscle (*Mapk14*$^{MCK\text{-}cre}$; p38α$^{MCK\text{-}KO}$ in the text). To generate double-KO mice for p38α and p38γ, we crossed p38α$^{MCK\text{-}KO}$ mice with whole-body KO mice for p38γ (B6.129-Mapk12^{tm1}), generating mice with whole-body deletion of p38γ and striated-muscle deletion of p38α (p38α/γ$^{MCK\text{-}KO}$ in the text). All animal procedures conformed to European Union Directive 2010/63/EU and Recommendation 2007/526/EC regarding the protection of animals used for experimental and other scientific purposes, enforced in Spanish law under Real Decreto 53/2013. All experiments were approved by the Spanish National Center for Cardiovascular Research (CNIC) Animal Care and Use Committee and the Community of Madrid. The protocol code is PROEX 215/18.

Mice were backcrossed for at least 10 generations to the C57BL/6N background and genotyped by PCR analysis of genomic DNA isolated from mouse tails. All studies were performed with male mice (8 to 29 weeks old). Mice were housed randomly in a pathogen-free animal facility and maintained on a 12-hour light/dark cycle at constant temperature and humidity. Mice were fed an ND (breeding and maintenance diets: D183, SAFE; and 1410, Altromin) or an HFD (HFD with 60% kcal fat and 1.5% cholesterol: D11103002i, Research Diets Inc.) ad libitum. HFD feeding started at 8 weeks of age.

Determination of energy balance

To determine energy expenditure, food intake, locomotor activity, wheel distance, wheel speed, and RQ, animals were placed in a custom-made 12 cage indirect calorimetry system for monitoring food intake and locomotor activity (TSE LabMaster, TSE Systems; Panlab, Harvard Apparatus and Sable Systems) (*39*). Mice were acclimatized to the metabolic cages for 48 hours and were then monitored for a further 48 hours. The indirect calorimetry system collected information about food intake, locomotor activity, wheel distance, wheel speed, and respiratory gas exchange [oxygen consumption, vO_2, and carbon dioxide production (vCO_2)] every 30 min. Reported results for all parameters were calculated from data collected throughout the second 48-hour period. RQ was calculated as the ratio of vCO_2 produced to vO_2 consumed (vCO_2/vO_2), thus determining the preferential macronutrient oxidation. Energy expenditure was calculated from O_2 consumption and CO_2 production measurements using standard analysis software provided with the calorimeter system. Locomotor activity was determined with infrared sensors that register horizontal and vertical movements.

Temperature measurement

Body temperature was measured with a rectal thermometer (AZ 8851 K/J/T Handheld Digital Thermometer-Single from AZ Instruments Corp. or a BAT-12 Microprobe Thermometer from Physitemp). For the determination of interscapular temperature as an index of BAT temperature, mice were shaved in the interscapular region, and images were captured with a thermographic camera (E60bx: Compact Infrared Thermal Imaging Camera, FLIR). Images were analyzed with FLIR Tools software.

For the cold exposure test, body temperature was measured with a rectal thermometer (BAT 12 Microprobe Thermometer, Physitemp), and mice were placed in a cold room at 4°C. Rectal temperature was measured every 60 min, with the last measurement made 6 hours after the beginning of the test.

In vivo metabolic tests

Glucose tolerance tests (GTTs), ITTs, and insulin release tests were performed as described (*40*). For GTT, mice were fasted overnight (16 hours), and basal glucose concentration was measured in tail-tip blood with a glucometer (Ascensia BREEZE 2 or Ascensia Contour Next One). Mice were then injected intraperitoneally with D-(+)-glucose monohydrate (Merck) dissolved in phosphate-buffered saline (PBS), and blood glucose concentration was measured at 15, 30, 60, 90, and 120 min after injection. For ITT, mice were fed ad libitum, and baseline glucose concentration was measured as for GTT. Mice were then injected intraperitoneally with insulin (0.75 U/kg body weight) (Lilly). Blood glucose concentration was measured at 15, 30, 60, 90, and 120 min after insulin injection and was expressed as a percentage of the baseline value. For the insulin release test, mice were fasted overnight (16 hours), and 100 µl of blood was collected from the submandibular vein in EDTA blood collection tubes (Microvette). Mice were then injected intraperitoneally with glucose (2 g/kg), and 100 µl of blood samples was collected using the same procedure 10 and 30 min after glucose injection. Plasma samples were obtained by centrifuging blood samples at 9600*g* for 20 min at 4°C.

Homeostasis model assessment of insulin resistance

The HOMA-IR was calculated as described (*40*). Glucose and insulin concentrations obtained after 16 hours of food withdrawal were measured and fed into the following formula

$$\frac{\text{Fasting blood glucose (mg / dl)} \times \text{Fasting insulin (µU / ml)}}{405}$$

Tail suspension test

The tail suspension test was performed as described (*41*) with minor modifications. Mice were acclimatized to the experimental room for 15 min. Mice were placed in a custom-made white tail suspension box measuring 42-cm high by 56-cm wide by 17.5-cm deep, which was divided into four three-walled rectangular compartments (42 cm-high by 14-cm wide by 17.5-cm deep) to prevent the mice from observing other animals. A suspension bar (1 cm-high by 1-cm wide by 60-cm long) was placed on the top of the box. The end of the mouse's tail was attached to the suspension bar in a parallel arrangement using a 17-cm tape. Hollow cylinders (4-cm long, 1.6-cm outside diameter, 1.2-cm inside diameter, 4.15 g) were placed around the mouse tails to prevent climbing behavior. Mice were suspended by the tail in the middle of their compartments, with the nose at an approximate height of 15 cm above the apparatus floor. Video recordings were made with digital camera over 6-min sessions, with four mice tested simultaneously. On-screen stopwatch software (Xnote Stopwatch, dnSoft Research Group) was used to measure mobility time for each mouse; small movements confined to the front legs and oscillations due to momentum gained during earlier movements were considered immobility and were excluded. Immobility time was calculated by subtracting the mobility time from the total 6 min of the session. All analysts were blinded to experimental group.

Treadmill exercise

ND-fed mice (7 to 8 weeks old) were exercised for 30 min by forced treadmill running at 10 cm/s for 5 min, 15 cm/s for 20 min, and 20 cm/s for 5 min, with the treadmill at a 10° uphill incline (five-lane LE8710 treadmill, Harvard Apparatus, Panlab) (*42*, *43*). The intensity of electrical stimulation was 0.2 mA. The same exercise protocol was repeated 2 days later. Blood was obtained from the submandibular vein immediately after exercise and collected in EDTA blood collection tubes (Microvette). Plasma was obtained after centrifugation at 9600*g* for 20 min at 4°C.

For the treadmill exhaustion test, acclimated mice to the LE405 treadmill (Harvard Apparatus, Panlab) were subjected with 10° inclination to the following protocol: 5 min at 10 cm/s, 5 min at 15 cm/s, 5 min at 20 cm/s, 5 min at 25 cm/s, and 3 cm/s more every 3 min until the mouse was exhausted (more than 3 s standing on the electrical shock grid set at 0.2 mA) (*44*). The investigator was blinded to the mouse genotype. Running speed, time, and distance were recorded. Work was calculated as previously described (*45*).

Endurance exercise training

ND-fed mice (7 to 8 weeks old) swam in 25-cm deep water in a glass container (60 cm by 30 cm by 45 cm) at 30° to 32°C for 5 weeks. The animals were progressively familiarized with swimming training over the first 2 weeks by increasing each swimming session by 10 min per day. Sessions were then maintained at 90 min until the end of the training. The first swimming session started at 12.30 p.m., and sessions were followed by 4 hours of rest. Mice were allowed to swim at their own pace, and the water was gently bubbled to ensure that mice swam rather than floating. The details of the protocol are detailed in Table 2.

Table 2. Endurance swimming exercise training protocol.

	Time [min (′)]						
Week 1	10′ + 10	20′ + 20′	30′ + 30′	40′ + 40′	50′ + 50′	0	0
Week 2	60′ + 60′	70′ + 70′	80′ + 80′	90′ + 90′	90′ + 90′	90′ + 90′	90′ + 90′
Week 3	90′ + 90′	90′ + 90′	90′ + 90′	90′ + 90′	90′ + 90′	90′ + 90′	90′ + 90′
Week 4	90′ + 90′	90′ + 90′	90′ + 90′	90′ + 90′	90′ + 90′	90′ + 90′	90′ + 90′
Week 5	90′ + 90′	90′ + 90′	90′ + 90′	90′ + 90′	End		

Open field

The apparatus of open field was a square white plastic box (40 cm by 40 cm by 40 cm) from Panlab (Harvard Apparatus). Mice were placed in the center region of the open field, and their movements were recorded for 7 min by videotaping from above. Videos were analyzed by AnyMaze software and total moving distance, mobile time, speed, and the time spent in the periphery, inner, or central region of the field were quantified. The apparatus was cleaned with 70% ethanol and air-dried before being used for another mouse.

Balance beam assay

The balance beam assay was carried out on a custom-built behavioral setup consisting of 2 beams of 80 cm of length and flat surfaces of 12- and 5-mm width, respectively, and resting 50 cm above the table top on two poles. Mice were subjected to three trials per day with the 12- and 5-mm beam, with 10- to 15-min intervals between trials for three consecutive days. In each session, mice were placed at the starting point of the beam, and the time required to cross to the end of the beam was recorded by a videotape. The finish point is one of the ends of the beam wherein a black box is located. When mice reached the end of the beam, they were allowed to stay there for 15 s. After each acclimated session, mice were returned to their home cages. The number of slips and the time spent in crossing the beam were manually quantified by a blinded investigator. The beam and the box were cleaned with 70% ethanol and air-dried between animals.

Echocardiography

Mice were anesthetized by inhalation of isoflurane and oxygen (1.25 and 98.75%, respectively), and echocardiography was performed with a 30-MHz transthoracic echocardiography probe. Images were obtained with the Vevo 2100 micro-ultrasound imaging system (VisualSonics, Toronto, Canada). Short-axis, long-axis, B-mode, and two-dimensional M-mode views were captured. Scans were performed by two experienced researchers who were blinded to the mouse genotype. Measurements of left parasternal long and short axes and M-mode images (left parasternal short axis) were taken at a heart rate of 500 to 550 beats per minute. Left ventricle (LV) end-diastolic diameter (LVEDD), LV end-systolic diameter (LVESD), and wall thickness were derived from M-mode tracings, and the average of three consecutive cardiac cycles was recorded. LV fractional shortening percentage was calculated as [(LVEDD − LVESD)/LVEDD] × 100. Lung MRI was conducted using a 7-T Agilent scanner equipped with a DD2 console and an actively shielded gradient set (205/120 insert of a maximum gradient strength of 130 mT m^{-1}). Signal-to-noise ratio during image acquisition was enhanced using a combination of a 72-mm–inner diameter quadrature birdcage TX volume coil and an actively detuning 30-mm flexible customized surface RX coil. Following the acquisition of a tripilot gradient-echo image, oblique coronal slices (1 to 2 slices) and axial slices (7 to 10 slices covering the entire lung) were obtained using specific parameters. These images facilitated the determination of interventricular septum and LV posterior wall thicknesses, as well as LV corrected mass; short-axis M-mode quantification was chosen as the most representative. Cardiac function was estimated from ejection fraction and fractional shortening obtained from M-mode views by a blinded echocardiography expert. Ejection fraction measurements were obtained from long- or short-axis views of the heart, with M-mode registration performed in a line perpendicular to the left ventricular septum and posterior wall at the level of the mitral chordae tendineae. The images were transferred to a computer and analyzed offline using the Vevo 2100 Workstation software.

Lentivirus vector production and stereotaxic microinjections

Lentiviruses were produced as described (*46*) with some modifications. Human embryonic kidney (HEK)–293 T cells were plated at 25 to 35% confluence in Dulbecco's modified Eagle medium (Gibco) supplemented with 10% fetal bovine serum (Sigma-Aldrich), 200 mM L-glutamine (Lonza), and penicillin/streptomycin (10,000 U/ml; 1:1; Lonza). HEK-293 T cells were transiently co-transfected using the calcium phosphate method with the pGIPZ empty vector or shRNAs against the IL-15 receptor α subunit (pGIPZ.shIL15Rα vector, V3LMM_451921, Dharmacon) together with the pΔ8.9 and pVSV-G packaging plasmids. Supernatants containing the lentiviral particles were collected 48 hours after removal of the calcium phosphate precipitate, filtered through 0.45-μm filters, and concentrated by ultracentrifugation at 115,500*g* for 2 hours at 4°C (Ultra-Clear Tubes, SW28 rotor and Optima L-100 XP Ultracentrifuge; Beckman Coulter).

Mice received injections in the primary motor cortex (M1) of 1 μl of lentiviral particles suspended in sterile PBS at a rate of 100 nl/min. Mice were placed in a stereotaxic frame (World Precision Instruments) under ketamine-xylazine anesthesia [intraperitoneally injected with 42.5% ketamine (Richter Pharma AG) and 20% xylazine hydrochloride (Bayer) in NaCl]. A longitudinal incision was made in the skin above the cranium, and lentiviruses were injected stereotaxically into the M1 area with a 32-gauge needle (Hamilton) connected to a 1-μl syringe. The following coordinates were used to reach the M1 area: anterior to the bregma, +1.1 mm; lateral to the sagittal suture, ±1.2 mm; and ventral to the skull surface, −1.5 mm. The incision was closed with sutures, and buprenorphine (0.1 mg/kg body weight) (Richter Pharma AG) was injected intraperitoneally after surgery as a painkiller.

Tail vein injection

WT male mice (weight, 20 to 25 g; age, 8 to 10 weeks old) were used and were held in a specific restrainer for tail vein injections. Mice were injected intravenously with 200 μl of IL-15 diluted in water (500 pg per mice; PeproTech, catalog no. 210-15). To overexpress p38γ specifically in the muscle, we designed an adenovirus (AAV-sk-cm4-cherry-p38γ*) in accordance with the previously outlined methodology (*47*). Subsequently, we administered the designed adenovirus, along with a control containing shScramble, intravenously at a dosage of 5×10^{11}.

Blood and organ collection

At sacrifice, blood samples were obtained from the submandibular vein and collected in EDTA blood collection tubes (Microvette), and plasma was obtained after centrifugation at 9600*g* for 20 min at 4°C. For most experiments, mice were fasted overnight, euthanized by cervical dislocation, and organs were removed, weighed using a precision balance and frozen in liquid nitrogen. For insulin signaling analysis, mice were injected intraperitoneally with insulin (1.5 U/kg; Lilly) 15 min before organ removal. Liver samples were collected in 10% formalin (Bio Optica) for H&E staining or frozen on dry ice after being embedded in optimal cutting temperature (OCT) compound (Tissue-Tek) for Oil Red staining. Brain samples were frozen on dry ice to preserve anatomy. The primary and secondary motor cortices (M1 and M2) were removed from the brain by cutting the caudal part of the hippocampus parallel to the base of the hypothalamus and 1.2 mm lateral to each side of the corpus callosum. The isolated sections were ~1-mm thick, in line with the Allen Brain reference Atlas (*48*).

Plasma analysis

Plasma insulin concentrations were measured by magnetic bead–based multiplex assay (Bio-Rad) with a Luminex 200 analyzer. IL-15 was detected in plasma samples by Western blot. Samples were diluted in PBS (1/5), Milli-Q water (H_2Omq), and Laemmli sample buffer and separated by SDS–polyacrylamide gel electrophoresis (PAGE) using AnykD Criterion TGX Precast gels (Bio-Rad).

Immunoblot analysis

From human muscle biopsies, ~10 mg of muscle was ground by stainless steel balls during 1 min in a Mikro-Dismembrator S (Sartorius, Goettingen, Germany) and immediately homogenized in urea lysis buffer (6 M urea, 1% SDS) and 50× Complete protease inhibitor (catalog no. 11697498001) and 10× PhosSTOP phosphatase inhibitor (catalog no. 4906837001) cocktails (Roche, Basel, Switzerland). Almost equal final concentration in all muscle protein extracts was acquired by following an individual adjustment of the extract volume using a volume calibration curve. Then, the lysate was centrifuged for 12 min at 25,200*g* at 16°C. The resulting supernatant was diluted with electrophoresis loading buffer [160 mM tris-HCl (pH 6.8), 5.9% SDS, 25.5% glycerol, and 15% β-mercaptoethanol-bromophenol blue] to achieve a similar concentration in all muscle lysates.

Mice tissue samples were homogenized with a T10 Ultra-Turrax (IKA) dispersing device in lysis buffer [50 mM tris-HCl (pH 7.5), 1 mM EGTA, 1 mM EDTA, 50 mM NaF, 1 mM sodium glycerophosphate, 5 mM sodium pyrophosphate, 0.27 M sucrose, 1% Triton X-100, 0.1% β-mercaptoethanol, 0.1 mM phenylmethylsulfonyl fluoride, 1 mM sodium orthovanadate, leupeptin (1 μg/ml), and aprotinin (1 μg/ml)]. Lysates were centrifuged at 19,000*g* for 20 min at 4°C, and protein concentration in supernatants was quantified by the Bradford method (Bio-Rad Protein Assay). Samples were denatured in loading buffer [0.24 M tris-HCl (pH 6.8), 40% glycerol, 8% SDS, 5% β-mercaptoethanol, and 0.04% bromophenol blue] at 95°C for 5 min. Equal protein amounts (20 to 50 μg) were loaded onto 10% polyacrylamide gels (30% acrylamide/bis solution, 29:1, Bio-Rad) or AnykD Criterion TGX Precast gels for IL-15 detection (Bio-Rad) and separated by SDS-PAGE. Gels were transferred to 0.2-μm–pore size nitrocellulose membranes (Bio-Rad) and blocked with 10% fat-free milk powder for 45 min. Membranes were probed overnight with primary antibodies against phospho-p38 (T180/Y182; 9211), phospho-p38γ (Invitrogen; PA5-105907), p38α (Santa Cruz Biotechnology, sc-535), p38γ (2307), phospho-MKK3 (S189)/MKK6 (S207) (9231), MKK3b (9238), MKK6 (Enzo Life Sciences; ADI-KAP-MA014-E), phospho-MK2 (T334; 3007), MK2 (3042), phospho-HSP27 (S82; 9709), phospho-AKT (T308; 2965), phospho-AKT (S473; 9271), AKT (9272), IL-15 (Abcam, ab273625), phospho-ERK1/2 (T202/Y204; 3101), ERK1/2 (9102), phospho-STAT3 (Y705; 9145), STAT3 (12640), phospho-STAT5 (Y694; 9359), STAT5 (94205), and vinculin (Sigma-Aldrich, V4505). All primary antibodies were used at 1:1000, except from anti-vinculin (1:2000) and were obtained from Cell Signaling Technology unless otherwise indicated. After washes with PBS–0.1% Tween, membranes were incubated for 1 hour at room temperature with horseradish peroxidase–conjugated goat anti-rabbit and sheep anti-mouse secondary antibodies (GE Healthcare) (1:5000). After further washes, reactive bands were detected by enhanced chemiluminescence (GE Healthcare) and quantified with ImageJ software (National Institutes of Health). In certain instances, membranes probed for phospho-proteins were stripped by incubation at 55°C for 15 min in stripping buffer [68 mM tris-HCl (pH 6.8), 1% SDS, and 0.7% β mercaptoethanol] and reprobed for the corresponding total protein. Phospho-protein amounts were normalized to the corresponding total protein.

RNA isolation and RT-qPCR

RNA from gastrocnemius samples was extracted with the RNeasy Fibrous Tissue Mini kit (QIAGEN). Muscle samples were dispersed with a T10 Ultra-Turrax (IKA) dispersing device. RNA concentration was measured with a NanoDrop 1000 spectrophotometer (Thermo Fisher Scientific). Between 200 ng and 1 μg of RNA were retrotranscribed using the High-Capacity cDNA Reverse Transcription Kit (Applied Biosystems). The following program was used: 10 min at 25°C, 2 hours at 37°C, and 5 min at 85°C. Samples were diluted 1:5, and mRNA expression was examined by real-time qPCR (RT-qPCR) using the 7900HT Fast Real-Time PCR System and FAST SYBR GREEN assays (Applied Biosystems). For RT-qPCR, 2 μl of diluted cDNA was added to 384 well MicroAmp Optical plates (Applied Biosystems) together with the following mix per well: 4 μl of the Fast SYBR Green Master Mix (Applied Biosystems), 0.16 μl of each primer, and 2 μl of ribonuclease (RNase)–free water. The plate included an eight-point standard curve created by fivefold serial dilution. SDS 2.4 software was used to run the following PCR program: one cycle of 20 s at 95°C plus 40 cycles of 1 s at 95°C and 20 s at 60°C. A dissociation curve was used after each reaction to verify primer specificity and PCR product purity. Relative mRNA expression was normalized to ribosomal protein S18 (Rps18) or glyceraldehyde-3-phosphate dehydrogenase (*Gapdh*) mRNA measured in each sample. The following genes were amplified using primers purchased from Sigma-Aldrich (F, forward; and R, reverse): *Map2k3*, F: GCCTCAGACCAAAGGAAAATCC and R:

GGTGTGGGGTTGGACACAG; *Map2k6*, F: ATGTCTCAGTCGAAAGGCAAG and R: TTGGAGTCTAAATCCCGAGGC; *Mapk12*, F: ATGCGCTACACGCAGACA and R: TGGTCATTGCCTTTGAACAG; *Rps18*, F: CAGCTCCAAGCGTTCCTGG and R: GGCCTTCAATTACAGTCGTCTTC; *Gapdh*, F: TGAAGCAGGCATCTGAGGG and R: CGAAGGTGGAAGAGTGGGA; and *Il15*, F: CATCCATCTCGTGCTACTTGTG and R: GCCTCTGTTTTAGGGAGACCT.

RNA-seq library preparation and sequencing and generation of FastQ files

Total RNA was isolated using the RNeasy Fibrous Tissue Mini Kit (QIAGEN) from gastrocnemius samples of mice fed a HFD for 6 weeks. RNA quality was verified using an Agilent 2100 Bioanalyzer, and individual samples with an RNA integrity number > 8 were included in the study. Two individual samples were pooled to obtain 200 ng of total RNA (100 ng from each pooled sample) in 100 μl of RNase-free water. RNA-seq was performed in the CNIC Genomics Unit. Total RNA was used to generate barcoded RNA-seq libraries using the NEBNext Ultra II Directional RNA Library preparation kit (New England Biolabs). First, poly A+ RNA was purified using poly-T oligo-attached magnetic beads followed by fragmentation and the first and second cDNA strand synthesis. Next, cDNA ends were repaired and adenylated. The NEBNext adaptor was then ligated, followed by second strand removal, uracile excision from the adaptor, and PCR amplification. The size of the libraries was checked using the Agilent 2100 Bioanalyzer, and concentration was determined with a Qubit fluorometer (Thermo Fisher Scientific). Libraries were sequenced on a HiSeq2500 System (Illumina) to generate 60-base single reads. FastQ files for each sample were obtained using CASAVA v1.8 software (Illumina).

RNA-seq data were analyzed by the CNIC Bioinformatics Unit. The number of reads per sample was between 25 million and 30 million. After assessing read quality with FastQC (*49*), reads were mapped against the GRCm38.76 mouse transcriptome, and gene expression levels were estimated with RNA-seq by Expectation Maximization (*50*). The "strandedness reverse" parameter was included to calculate expression from directional RNA-seq data. The percentage of aligned reads was between 91 and 94% for all samples. Expression count matrices were then processed with an analysis pipeline that used the Bioconductor package limma (*51*) for normalization (using trimmed mean of M-value method) and differential expression testing, taking into account only those genes expressed with at least one count per million in at least three samples (the number of samples available for each condition). Three pairwise contrasts were performed: $p38\alpha^{MCK\text{-}KO}$ versus control, $p38\alpha/\gamma^{MCK\text{-}KO}$ versus control, and $p38\alpha^{MCK\text{-}KO}$ versus $p38\alpha/\gamma^{MCK\text{-}KO}$. Changes in gene expression were considered significant if associated with a Benjamini and Hochberg adjusted *P* value of <0.05.

Histological analysis

Liver tissue samples were fixed for 48 hours in 10% formalin (Bio-Optica), dehydrated, and embedded in paraffin. Sections (8 μm) were cut and stained with H&E (American Master Tech Scientific). For Oil Red staining, 8-μm sections were prepared from tissue frozen in OCT compound (Tissue-Tek) using a cryostat (Leica CM 1950). Sections were fixed in 10% formalin (Bio-Optica) for 10 min at 4°C and rinsed with distilled water. Sections were immersed in propylene glycol (Sigma-Aldrich) for 5 min at room temperature, changed to propylene glycol, and left for a further 5 min. Samples were stained for 10 min with pre-warmed (60°C) Oil Red O solution (7 mg/ml; Oil Red O from Sigma-Aldrich in propylene glycol). Propylene glycol (85%) was added for 3 min, and samples were rinsed in distilled water and embedded in hematoxylin for 1 min, washed in water, and introduced into Bluing solution. Sections were then washed in tap water, rinsed in distilled water, and mounted in Aquatex aqueous mounting agent (Merck).

All samples were examined with a Leica DM2500 microscope at various magnifications and imaged using Leica Application Suite v4.3 (LAS v4.3). For histological examination of skeletal muscles, samples were immediately frozen in liquid nitrogen–cooled isopentane (2-methylbutane, Sigma-Aldrich) following extraction and kept on dry ice until lastly stored at −80°C. Muscle samples were cut into 8-μm-thick cryosections with a cryostat (Leica CM 1950) on microscope slides (Superfrost Plus, Thermo Fisher Scientific) maintained at −20°C and incubated with the antibody rabbit anti-DsRed (Living colours; ref. 632496, Clontech) 4°C overnight. Three consecutive washes with PBS–Triton X-100 (0.1%) and one with PBS at room temperature for 5 min each were followed by sequential incubation with Alexa Fluor 546–conjugated secondary antibody (Invitrogen) at room temperature for 1 hour in the dark. Muscle sections were then washed three times with PBS–Triton X-100 (0.1%) and once with PBS at room temperature for 5 min each. Slides were mounted in VECTASHIELD mounting medium (Palex) and visualized with a Leica TCS-SP5 confocal at ×20 magnification.

Identification of secreted proteins

Potential p38γ-induced genes were identified by gene expression analysis comparing muscles from $p38\alpha^{MCK\text{-}KO}$ or $p38\alpha/\gamma^{MCK\text{-}KO}$ mice with controls, and all candidates with a *P* value of <0.05 were filtered for those encoding secreted proteins using the SignalP, SecretomeP, and TargetP programs (www.cbs.dtu.dk/services/) (*52*). Heatmap representations were created using the Heatmapper tool.

Statistics

Values are presented as means ± SEM. Differences between groups were examined for statistical significance by two-tailed unpaired Student's *t* test (with Welch's correction when variances were different) or one- or two-way analysis of variance (ANOVA) coupled to Bonferroni's posttest. Analysis of covariance for energy expenditure measurements was performed with body weight as the covariate using R software. Statistical significance was determined as a two-sided *P* value of <0.05 (GraphPad Prism 8.0). Family-wise error rate *P* values are displayed for GSEA to correct for multiple hypothesis testing. Statistical details and experimental *n* are specified in figure legends.

Supplementary Materials

This PDF file includes:
Figs. S1 to S8
Legends for data S1 and S2

Other Supplementary Material for this manuscript includes the following:
Data S1 and S2

REFERENCES AND NOTES

1. World Health Organization (WHO), "Obesity and overweight" (WHO, 2020); www.who.int/news-room/fact-sheets/detail/obesity-and-overweight.

2. B. N. Greenwood, T. E. Foley, T. V. Le, P. V. Strong, A. B. Loughridge, H. E. Day, M. Fleshner, Long-term voluntary wheel running is rewarding and produces plasticity in the mesolimbic reward pathway. *Behav. Brain Res.* **217**, 354–362 (2011).
3. M. M. Atakan, S. N. Kosar, Y. Guzel, H. T. Tin, X. Yan, The role of exercise, diet, and cytokines in preventing obesity and improving adipose tissue. *Nutrients* **13**, 1459 (2021).
4. C. Priest, P. Tontonoz, Inter-organ cross-talk in metabolic syndrome. *Nat. Metab.* **1**, 1177–1188 (2019).
5. L. S. Chow, R. E. Gerszten, J. M. Taylor, B. K. Pedersen, H. van Praag, S. Trappe, M. A. Febbraio, Z. S. Galis, Y. Gao, J. M. Haus, I. R. Lanza, C. J. Lavie, C. H. Lee, A. Lucia, C. Moro, A. Pandey, J. M. Robbins, K. I. Stanford, A. E. Thackray, S. Villeda, M. J. Watt, A. Xia, J. R. Zierath, B. H. Goodpaster, M. P. Snyder, Exerkines in health, resilience and disease. *Nat. Rev. Endocrinol.* **18**, 273–289 (2022).
6. S. Rodríguez-Fdez, L. F. Lorenzo-Martín, I. Fernández-Pisonero, B. Porteiro, C. Veyrat-Durebex, D. Beiroa, O. Al-Massadi, A. Abad, C. Diéguez, R. Coppari, R. Nogueiras, X. R. Bustelo, Vav2 catalysis-dependent pathways contribute to skeletal muscle growth and metabolic homeostasis. *Nat. Commun.* **11**, 5808 (2020).
7. B. K. Pedersen, M. A. Febbraio, Muscles, exercise and obesity: Skeletal muscle as a secretory organ. *Nat. Rev. Endocrinol.* **8**, 457–465 (2012).
8. A. Combes, J. Dekerle, N. Webborn, P. Watt, V. Bougault, F. N. Daussin, Exercise-induced metabolic fluctuations influence AMPK, p38-MAPK and CaMKII phosphorylation in human skeletal muscle. *Physiol. Rep.* **3**, e12462 (2015).
9. C. de Alvaro, T. Teruel, R. Hernandez, M. Lorenzo, Tumor necrosis factor alpha produces insulin resistance in skeletal muscle by activation of inhibitor kappaB kinase in a p38 MAPK-dependent manner. *J. Biol. Chem.* **279**, 17070–17078 (2004).
10. I. Nikolic, M. Leiva, G. Sabio, The role of stress kinases in metabolic disease. *Nat. Rev. Endocrinol.* **16**, 697–716 (2020).
11. A. R. Pogozelski, T. Geng, P. Li, X. Yin, V. A. Lira, M. Zhang, J. T. Chi, Z. Yan, p38gamma mitogen-activated protein kinase is a key regulator in skeletal muscle metabolic adaptation in mice. *PLOS ONE* **4**, e7934 (2009).
12. S. E. Kahn, R. L. Hull, K. M. Utzschneider, Mechanisms linking obesity to insulin resistance and type 2 diabetes. *Nature* **444**, 840–846 (2006).
13. A. Cuenda, P. Cohen, V. Buée-Scherrer, M. Goedert, Activation of stress-activated protein kinase-3 (SAPK3) by cytokines and cellular stresses is mediated via SAPKK3 (MKK6); comparison of the specificities of SAPK3 and SAPK2 (RK/p38). *EMBO J.* **16**, 295–305 (1997).
14. B. Gonzalez-Teran, N. Matesanz, I. Nikolic, M. A. Verdugo, V. Sreeramkumar, L. Hernandez-Cosido, A. Mora, G. Crainiciuc, M. L. Saiz, E. Bernardo, L. Leiva-Vega, E. Rodriguez, V. Bondia, J. L. Torres, S. Perez-Sieira, L. Ortega, A. Cuenda, F. Sanchez-Madrid, R. Nogueiras, A. Hidalgo, M. Marcos, G. Sabio, p38γ and p38δ reprogram liver metabolism by modulating neutrophil infiltration. *EMBO J.* **35**, 536–552 (2016).
15. A. Koh, A. Molinaro, M. Ståhlman, M. T. Khan, C. Schmidt, L. Mannerås-Holm, H. Wu, A. Carreras, H. Jeong, L. E. Olofsson, P. O. Bergh, V. Gerdes, A. Hartstra, M. de Brauw, R. Perkins, M. Nieuwdorp, G. Bergstrom, F. Bäckhed, Microbially produced imidazole propionate impairs insulin signaling through mTORC1. *Cell* **175**, 947–961.e17 (2018).
16. J. D. Crane, L. G. MacNeil, J. S. Lally, R. J. Ford, A. L. Bujak, I. K. Brar, B. E. Kemp, S. Raha, G. R. Steinberg, M. A. Tarnopolsky, Exercise-stimulated interleukin-15 is controlled by AMPK and regulates skin metabolism and aging. *Aging Cell* **14**, 625–634 (2015).
17. Y. He, X. Wu, R. S. Khan, A. J. Kastin, G. G. Cornelissen-Guillaume, H. Hsuchou, B. Robert, F. Halberg, W. Pan, IL-15 receptor deletion results in circadian changes of locomotor and metabolic activity. *J. Mol. Neurosci.* **41**, 315–321 (2010).
18. E. E. Pistilli, S. Bogdanovich, F. Garton, N. Yang, J. P. Gulbin, J. D. Conner, B. G. Anderson, L. S. Quinn, K. North, R. S. Ahima, T. S. Khurana, Loss of IL-15 receptor α alters the endurance, fatigability, and metabolic characteristics of mouse fast skeletal muscles. *J. Clin. Invest.* **121**, 3120–3132 (2011).
19. M. Nalbandian, M. Zhao, H. Kato, T. Jonouchi, M. Nakajima-Koyama, T. Yamamoto, H. Sakurai, Single-cell RNA-seq reveals heterogeneity in hiPSC-derived muscle progenitors and E2F family as a key regulator of proliferation. *Life Sci. Alliance* **5**, e202101312 (2022).
20. B. K. Pedersen, Physical activity and muscle-brain crosstalk. *Nat. Rev. Endocrinol.* **15**, 383–392 (2019).
21. X. Wu, Y. He, H. Hsuchou, A. J. Kastin, J. C. Rood, W. Pan, Essential role of interleukin-15 receptor in normal anxiety behavior. *Brain Behav. Immun.* **24**, 1340–1346 (2010).
22. X. Wu, H. Hsuchou, A. J. Kastin, Y. He, R. S. Khan, K. P. Stone, M. S. Cash, W. Pan, Interleukin-15 affects serotonin system and exerts antidepressive effects through IL15Rα receptor. *Psychoneuroendocrinology* **36**, 266–278 (2011).
23. S. Grillner, A. El Manira, Current principles of motor control, with special reference to vertebrate locomotion. *Physiol. Rev.* **100**, 271–320 (2020).
24. A. Gallego-Selles, M. Martin-Rincon, M. Martinez-Canton, M. Perez-Valera, S. Martín-Rodríguez, M. Gelabert-Rebato, A. Santana, D. Morales-Alamo, C. Dorado, J. A. L. Calbet, Regulation of Nrf2/Keap1 signalling in human skeletal muscle during exercise to exhaustion in normoxia, severe acute hypoxia and post-exercise ischaemia: Influence of metabolite accumulation and oxygenation. *Redox Biol.* **36**, 101627 (2020).
25. Y. Tamura, K. Watanabe, T. Kantani, J. Hayashi, N. Ishida, M. Kaneki, Upregulation of circulating IL-15 by treadmill running in healthy individuals: Is IL-15 an endocrine mediator of the beneficial effects of endurance exercise? *Endocr. J.* **58**, 211–215 (2011).
26. A. R. Nielsen, R. Mounier, P. Plomgaard, O. H. Mortensen, M. Penkowa, T. Speerschneider, H. Pilegaard, B. K. Pedersen, Expression of interleukin-15 in human skeletal muscle effect of exercise and muscle fibre type composition. *J. Physiol.* **584**, 305–312 (2007).
27. A. R. Nielsen, P. Hojman, C. Erikstrup, C. P. Fischer, P. Plomgaard, R. Mounier, O. H. Mortensen, C. Broholm, S. Taudorf, R. Krogh-Madsen, B. Lindegaard, A. M. Petersen, J. Gehl, B. K. Pedersen, Association between interleukin-15 and obesity: Interleukin-15 as a potential regulator of fat mass. *J. Clin. Endocrinol. Metab.* **93**, 4486–4493 (2008).
28. H. Sun, Y. Ma, M. Gao, D. Liu, IL-15/sIL-15Rα gene transfer induces weight loss and improves glucose homeostasis in obese mice. *Gene Ther.* **23**, 349–356 (2016).
29. H. Sun, D. Liu, Hydrodynamic delivery of interleukin 15 gene promotes resistance to high fat diet-induced obesity, fatty liver and improves glucose homeostasis. *Gene Ther.* **22**, 341–347 (2015).
30. L. Nguyen, J. Bohlen, J. Stricker, I. Chahal, H. Zhang, E. E. Pistilli, Hippocampus-specific deficiency of IL-15Rα contributes to greater anxiety-like behaviors in mice. *Metab. Brain Dis.* **32**, 297–302 (2017).
31. N. Matesanz, I. Nikolic, M. Leiva, M. Pulgarín-Alfaro, A. M. Santamans, E. Bernardo, A. Mora, L. Herrera-Melle, E. Rodríguez, D. Beiroa, A. Caballero, E. Martín-García, R. Acín-Pérez, L. Hernández-Cosido, L. Leiva-Vega, J. L. Torres, F. Centeno, A. R. Nebreda, J. A. Enríquez, R. Nogueiras, M. Marcos, G. Sabio, p38α blocks brown adipose tissue thermogenesis through p38δ inhibition. *PLOS Biol.* **16**, e2004455 (2018).
32. R. Romero-Becerra, A. Mora, E. Manieri, I. Nikolic, A. M. Santamans, V. Montalvo-Romeral, F. M. Cruz, E. Rodríguez, M. León, L. Leiva-Vega, L. Sanz, V. Bondía, D. Filgueiras-Rama, L. J. Jiménez-Borreguero, J. Jalife, B. Gonzalez-Teran, G. Sabio, MKK6 deficiency promotes cardiac dysfunction through MKK3-p38γ/δ-mTOR hyperactivation. *eLife* **11**, e75250 (2022).
33. D. Morales-Alamo, J. Losa-Reyna, R. Torres-Peralta, M. Martin-Rincon, M. Perez-Valera, D. Curtelin, J. G. Ponce-González, A. Santana, J. A. Calbet, What limits performance during whole-body incremental exercise to exhaustion in humans? *J. Physiol.* **593**, 4631–4648 (2015).
34. M. Martin-Rincon, M. Gelabert-Rebato, M. Perez-Valera, V. Galvan-Alvarez, D. Morales-Alamo, C. Dorado, R. Boushel, J. Hallen, J. A. L. Calbet, Functional reserve and sex differences during exercise to exhaustion revealed by post-exercise ischaemia and repeated supramaximal exercise. *J. Physiol.* **599**, 3853–3878 (2021).
35. M. Martin-Rincon, J. J. González-Henríquez, J. Losa-Reyna, I. Perez-Suarez, J. G. Ponce-González, J. de La Calle-Herrero, M. Perez-Valera, A. Pérez-López, D. Curtelin, E. D. Cherouveim, D. Morales-Alamo, J. A. L. Calbet, Impact of data averaging strategies on $\dot{V}O_{2max}$ assessment: Mathematical modeling and reliability. *Scand. J. Med. Sci. Sports* **29**, 1473–1488 (2019).
36. I. Perez-Suarez, M. Martin-Rincon, J. J. Gonzalez-Henriquez, C. Fezzardi, S. Perez-Regalado, V. Galvan-Alvarez, J. W. Juan-Habib, D. Morales-Alamo, J. A. L. Calbet, Accuracy and precision of the COSMED K5 portable analyser. *Front. Physiol.* **9**, 1764 (2018).
37. B. Guerra, M. C. Gómez-Cabrera, J. G. Ponce-González, V. E. Martinez-Bello, A. Guadalupe-Grau, A. Santana, V. Sebastia, J. Viña, J. A. L. Calbet, Repeated muscle biopsies through a single skin incision do not elicit muscle signaling, but IL-6 mRNA and STAT3 phosphorylation increase in injured muscle. *J. Appl. Physiol.* **110**, 1708–1715 (2011).
38. L. Hui, L. Bakiri, A. Mairhorfer, N. Schweifer, C. Haslinger, L. Kenner, V. Komnenovic, H. Scheuch, H. Beug, E. F. Wagner, p38alpha suppresses normal and cancer cell proliferation by antagonizing the JNK-c-Jun pathway. *Nat. Genet.* **39**, 741–749 (2007).
39. T. A. Czyzyk, R. Nogueiras, J. F. Lockwood, J. H. McKinzie, T. Coskun, J. E. Pintar, C. Hammond, M. H. Tschöp, M. A. Statnick, κ-Opioid receptors control the metabolic response to a high-energy diet in mice. *FASEB J.* **24**, 1151–1159 (2010).
40. G. Sabio, J. Cavanagh-Kyros, H. J. Ko, D. Y. Jung, S. Gray, J. Y. Jun, T. Barrett, A. Mora, J. K. Kim, R. J. Davis, Prevention of steatosis by hepatic JNK1. *Cell Metab.* **10**, 491–498 (2009).
41. A. Can, D. T. Dao, C. E. Terrillion, S. C. Piantadosi, S. Bhat, T. D. Gould, The tail suspension test. *J. Vis. Exp.* **2012**, e3769 (2012).
42. B. Castro, S. Kuang, Evaluation of muscle performance in mice by treadmill exhaustion test and whole-limb grip strength assay. *Bio. Protoc.* **7**, e2237 (2017).
43. J. P. Dougherty, D. A. Springer, M. C. Gershengorn, The treadmill fatigue test: A simple, high-throughput assay of fatigue-like behavior for the mouse. *J. Vis. Exp.* **2016**, 54052 (2016).
44. S. Lebek, X. M. Caravia, L. G. Straub, D. Alzhanov, W. Tan, H. Li, J. R. McAnally, K. Chen, L. Xu, P. E. Scherer, N. Liu, R. Bassel-Duby, E. N. Olson, CRISPR-Cas9 base editing of pathogenic CaMKIIδ improves cardiac function in a humanized mouse model. *J. Clin. Invest.* **134**, e175164 (2024).

45. Y. Nie, Y. Sato, C. Wang, F. Yue, S. Kuang, T. P. Gavin, Impaired exercise tolerance, mitochondrial biogenesis, and muscle fiber maintenance in miR-133a-deficient mice. *FASEB J.* **30**, 3745–3758 (2016).
46. K. Urso, A. Alfranca, S. Martínez-Martínez, A. Escolano, I. Ortega, A. Rodriguez, J. M. Redondo, NFATc3 regulates the transcription of genes involved in T-cell activation and angiogenesis. *Blood* **118**, 795–803 (2011).
47. S. Sarcar, W. Tulalamba, M. Y. Rincon, J. Tipanee, H. Q. Pham, H. Evens, D. Boon, E. Samara-Kuko, M. Keyaerts, M. Loperfido, E. Berardi, S. Jarmin, P. In't Veld, G. Dickson, T. Lahoutte, M. Sampaolesi, P. De Bleser, T. VandenDriessche, M. K. Chuah, Next-generation muscle-directed gene therapy by in silico vector design. *Nat. Commun.* **10**, 492 (2019).
48. Allen Institute for Brain Science, "Allen Mouse Brain Atlas" (Allen Institute for Brain Science, 2004); https://mouse.brain-map.org/static/atlas.
49. S. Andrews, "A quality control application for high throughput sequence data" (Babraham Institute, 2010); www.bioinformatics.babraham.ac.uk/projects/fastqc/.
50. B. Li, C. N. Dewey, RSEM: Accurate transcript quantification from RNA-Seq data with or without a reference genome. *BMC Bioinformatics* **12**, 323 (2011).
51. M. E. Ritchie, B. Phipson, D. Wu, Y. Hu, C. W. Law, W. Shi, G. K. Smyth, limma powers differential expression analyses for RNA-sequencing and microarray studies. *Nucleic Acids Res.* **43**, e47 (2015).
52. O. Emanuelsson, S. Brunak, G. von Heijne, H. Nielsen, Locating proteins in the cell using TargetP, SignalP and related tools. *Nat. Protoc.* **2**, 953–971 (2007).

Acknowledgments: We thank R. J. Davis (University of Massachusetts Medical School, Worcester, MA) for the shIL-15Rα plasmid. We thank E. F. Wagner (Medizinische Universität Wien, Austria) for the p38α flox mice. We thank S. Bartlett for English editing. G.S. is a Miembro Numerario of the RACVE. The technical assistance by J. Navarro de Tuero is appreciated. **Funding:** This work was supported by Ministerio de Educación, Cultura y Deporte (FPU15 05802) (L.H.-M.); Sara Borrell Instituto de Salud Carlos III (CD19/00078), EFSD/Lilly Young Investigator Award 2022, Society for Endocrinology/Early Career Grant 2022, FSEEN/Jóvenes endocrinólogos 2022/EFSD/Novo Nordisk Rising Star 2024 (CF); Proyectos I+D+i 2019 - Modalidades «Retos Investigación» y «Generación de Conocimiento» funded by Ministerio de Economía y Competitividad (MINECO-PID2019-104399RB-I00 (GS) and Proyectos de I+D de Generación de Conocimiento 2018 funded by Ministerio de Economía y Competitividad (PGC2018-097019-B-I00) (J.V.); PreMed-Exp: PMP21/00057, PMP21/00113 Infraestructura de Medicina de Precisión asociada a la Ciencia y Tecnología IMPACT-2021; Instituto de Salud Carlos III (G.S. and J.L.T.); Instituto de Salud Carlos III (ISCIII) and the European Union project PI20/00743 (M.M.); Carlos III Institute of Health-Fondo de Investigación Sanitaria grant PRB3 (PT17/0019/0003- ISCIII-SGEFI/ERDF, ProteoRed) (J.V.); Fundación Jesús Serra (G.S.); EFSD/Lilly European Diabetes Research Programme (G.S.); BBVA Foundation Leonardo Grants program for Researchers and Cultural Creators (Investigadores-BBVA-2017) (G.S.); Fundación AECC PROYE19047SABI (G.S.); Comunidad de Madrid IMMUNOTHERCAN-CM S2010/BMD-2326 (G.S.) and B2017/BMD-3733 (G.S.).; G.S. is a EMBO YIP member (G.S.); Agencia Estatal de Investigación (PID2022-138525OB-I00) funded by MICIU/AEI/10.13039/501100011033, FEDER funds, and the EU (G.S.); PDC2021-121147-I00.Convocatoria: Proyectos Prueba de Concepto 2021. Ministerio de Ciencia e Innovación (G.S.); "La Caixa" Banking Foundation (project code HR17-00247) (J.V.); Ministerio de Economía y Competitividad (DEP2015-71171-R; DEP2017-86409-C2-1-P) (J.A.L.C.) and ACIISI (ProID2017010106) (J.A.L.C.); the CNIC is supported by the Instituto de Salud Carlos III (ISCIII), the Ministerio de Ciencia e Innovación (MCIN), and the Pro CNIC Foundation and is a Severo Ochoa Center of Excellence (grant CEX2020-001041-S funded by MICIN/AEI/10.13039/501100011033). **Author contributions:** Conceptualization, develop the hypothesis and generate project resources: G.S., A.M., C.F., L.H.-M., B.M.S., J.A.L., J.A.L.C., J.V., M.M.-R., J.L.T., L.H.-C., and M.M. Methodology, perform the experiments, formal analysis, and prepare figures: L.H.-M., C.F., A.M., G.S., V.G.-A., B.M.S., J.A.L., M.M., J.A.L.C., M.Á.M., J.V., M.M.-R., and P.A.D. Investigation and assistance in experiments analysis: A.M., C.F., L.H.-M., G.S., J.A.L., E.R., A.G.-C., L.L.-V., B.P., M.L., C.I., C.B., and J.V. Investigation and provide human samples: M.M.-R., M.M., J.A.L.C., and L.H.-C. Visualization: A.M., G.S., C.F., L.H.-M., M.I.C., V.G.-A., and M.M.-R. Funding adquisition: C.F., G.S., M.M.-R., J.V., J.A.L.C., and M.M. Data curation: M.M.-R. Validation: A.M., G.S., C.F., L.H.-M., M.M.-R., M.Á.M., J.A.L.C., and V.G.-A. Project administration: A.M., G.S., C.F., M.M.-R., J.A.L.C., and M.M. Supervision: G.S., A.M., B.M.S., M.M.-R., M.Á.M., J.A.L.C., and M.M. Writing—original draft: G.S., A.M., L.H.-M., C.F., V.G.-A., and M.M.-R. Writing—review and editing: G.S., A.M., L.H.-M., C.F., V.G.-A., M.M.-R., B.M.S., J.A.L., M.M., A.G.-C., M.I.C., J.V., J.L.T., M.Á.M., L.H.-C., and P.A.D. **Competing interests:** The authors declare that they have no competing interest. **Data and materials availability:** All data needed to evaluate the conclusions in the paper are present in the paper and/or the Supplementary Materials. The material transfer agreement (MTA) can be provided by G.S. pending scientific review and a completed MTA. Requests for the MTA should be submitted to: GS.

Submitted 18 December 2023
Accepted 10 July 2024
Published 14 August 2024
10.1126/sciadv.adn5993